



EUROPEAN
COMMISSION

Community research

SEARCH

Safety ExploitAtion Related CHemistry for HLM reactors

(Contract Number: **295736**)

DELIVERABLE D5.3

Two-phase CFD model of the MYRRHA-FASTEF primary coolant loop including all relevant thermal aspects

Author: **V. Moreau (CRS4)**

Reporting period: **01/11/2011 – 30/04/2013**

Date of issue of this report: **04/12/2013**

Start date of project: **01/11/2011**

Duration: **36 Months**

Project co-funded by the European Commission under the Seventh Euratom Framework Programme for Nuclear Research & Training		
Dissemination Level		
PU	Public	X
RE	Restricted to a group specified by the partners of the SEARCH	
CO	Confidential, only for partners of the SEARCH project	

[SEARCH]



DISTRIBUTION LIST

Name	Institute	Comments
Bandini Giacomino	ENEA	Email notification of submission to the EC. Copy available on the SEARCH website.
Buchlin Jean-Marie	VKI	
Buckingham Sophia	VKI	
Chen Xue-Nong	KIT	
Class Andreas	KIT	
Cottenier Stefaan	UGENT	
Delville Rémi	SCK•CEN	
Di Piazza Ivan	ENEA	
Doolaard Heleen	NRG	
Eichler Robert	PSI	
Flad Michael	KIT	
Forgione Nicola	UNIFI	
Gessi Alessandro	ENEA	
Hania Ralph	NRG	
Heinitz Stephan	PSI	
Jayaraju Santhosh	NRG	
Kennedy Graham	SCK•CEN	
Koloszar Lilla	VKI	
Konings Rudy	JRC	
Konovalenko Alexander	KTH	
Li Rui	KIT	
Litfin Karsten	KIT	
Lucan Dumitra	INR	
Maschek Werner	KIT	
Matzerath Claudia	KIT	
Maugeri Emilio	PSI	
Moreau Vincent	CRS4	
Neuhausen Jörg	PSI	
Pellini Donella	KIT	
Planquart Philippe	VKI	
Raison Philippe	JRC	
Retegan Teodora	CHALMERS	
Rijpstra Kim	UGENT	
Rineiski Andrei	KIT	
Rizzi Matthias	PSI	
Roelofs Ferry	NRG	
Schroer Carsten	KIT	
Schumann Dorothea	PSI	
Schuurmans Paul	SCK•CEN	
Skarnemark Gunnar	CHALMERS	
Tarantino Mariano	ENEA	
Taufall Simon	KIT	
Van den Bosch Joris	SCK•CEN	
Van Speybroeck Veronique	UGENT	
Van Yperen-De Deyne Andy	UGENT	
Weisenburger Alfons	KIT	
Westlake Jonathan	NRG	
Wetzel Thomas	KIT	
Roger Garbil	EC	
European Comission Services		

[SEARCH]

SEARCH – Grant Agreement n° 295736

Safe ExploitAtion Related CHemistry for HLM reactors

EC project officer: Roger Garbil

Workpackage No:	WP5	Task No:	1
SEARCH Identification:	DEL5.3-2012	Revision:	0





Short description of revision:

Summary: Two CFD models of the primary coolant loop of MYRRHA revision 1.4 are described. The first one encompass all the primary LBE loop, the cover gas and the thermal interaction with the critical 100MW heat core production. The second incorporates also the main structural parts and its thermal interaction with the flow. Transient simulations, bringing the models close to the nominal operation , are described and discussed.

Title:

Two-phase CFD model of the MYRRHA-FASTEF primary coolant loop including all relevant thermal aspects

Dissemination level :	PU
Issued by:	CRS4
Internal reference by editing partner:	
Status:	Final

2013-12-04				
DATE	Author V. Moreau CRS4	Task leader V. Moreau CRS4	WP leader V. Moreau CRS4	Coordinator P. Schuurmans SCK•CEN

Abstract

The aim of this report is to describe the work performed to develop a comprehensive CFD representation of the MYRRHA primary loop. The structure of the CFD geometry is described as well as the physical modelling. The model includes the free surfaces dynamics of the LBE and is transient in nature. A simulation with 6 million control volumes and restricted to the fluid domain has been run, reaching nominal condition starting from the fluid at rest. The stability of the flow under nominal conditions is then been checked by monitoring the velocity and temperature field during 120s. It can be seen that under these conditions, the flow is quite well stabilized by the thermal stratification in the hot plenum. The flow in the cold plenum is not stationary but slowly oscillate around a mean configuration.

A second model, taking into account the conjugate heat transfer with the structural part has been built and simulated. The second model is slightly larger with 9.3 million cells, one of with for the structural part. The simulation has been monitored for 300s and the results of the monitoring are presented and discussed. While the characteristic solid heat transfer time scale is too long to reach back a global thermal equilibrium in an affordable time, the main circulation is only marginally affected. A slight instability of one of the two primary pumps is however observed.

LIST OF CONTENT

ABSTRACT	4
LIST OF CONTENT	4
NOMENCLATURE	6
1. INTRODUCTION	8
2. LIST OF 3D-CAD MODELS WITH GEOMETRICAL DESCRIPTION	10
2.1 Butterfly.....	10
2.2 Core Barrel	11
2.3 Core, IPS and SR layout	12
2.4 IVFS.....	14
2.5 Porous and Voids.....	15
2.6 Main Structure	16
2.6.1 Reactor Vessel	16
2.6.2 Heat eXchangers (HXs)	17
2.6.3 Base Solid (Diaphragm)	18
2.7 Numerical Top	22

[SEARCH]

2.8	Primary pumps	22
2.8.1	Pump chimney.....	22
2.8.2	Pump guide lower part.....	22
3.	CFD FLUID REGIONS	23
4.	PHYSICAL PROPERTIES.....	24
5.	MOMENTUM AND HEAT SOURCES	25
5.1	Core	25
5.1.1	Hydraulic resistance (as a force density).....	25
5.1.2	Core Heat source	26
5.2	PHX	27
5.2.1	PHX Heat source	27
5.2.2	PHX Hydraulic resistance.....	28
5.3	PP.....	29
6.	PHASE CONTROL	29
7.	TRANSIENT FLUID FLOW SIMULATION TO NOMINAL CONDITION	29
7.1	Numerical setting	30
7.2	Mass flow rates	31
7.3	Velocity field.....	32
7.4	Thermal field	33
7.5	Thermal balance.....	36
8.	CONJUGATE HEAT TRANSFER SIMULATION	37
8.1	Updated model	38
8.2	Results	39
8.2.1	Thermal field	40
8.2.2	Velocity field.....	44
9.	CONCLUDING WORD	46
	REFERENCES.....	47
	APPENDIX: LIST OF USER FUNCTIONS REPORTS AND PLOTS.....	47

NOMENCLATURE

Roman Letters

c specific heat [J/(kg K)]
 k_{∞} infinite multiplication factor

Greek Letters

α volume fraction [adim]
 ε Friction factor [adim]
 κ thermal conductivity [W/(m K)]
 μ dynamic viscosity [Pa s]
 ρ density [kg/m³]
 τ characteristic time constant [s]

Abbreviations and acronyms

3D	Three Dimensional
ADS	Accelerator Driven System
CAD	Computer Aided Design
CDA	Core Disruptive Accident
CFD	Computational Fluid Dynamic
CR	Control Rod
FA	Fuel Assembly
FASTEF	Fast Spectrum Transmutation Experimental Facility
FCI	Fuel Coolant Interaction
FP	Fission Product
FZK	Forschungszentrum Karlsruhe
HX	Heat eXchanger
IPS	In Pile Section
IVFH(M)	In Vessel Fuel Handling (Machine)
IVFS	In Vessel Fuel Storage
LBE	Lead Bismuth Eutectic
LFR	Lead Fast Reactor
LMFR	Liquid Metal Fast Reactor
MYRRHA	Multi-purpose hYbrid Research Reactor for High-tech Applications

[SEARCH]

Deliverable 5.3 – [Two-phase CFD model of the MYRRHA-FASTEF primary coolant loop including all relevant thermal aspects](#)

Dissemination level: [PU](#)

Date of issue of this report: [04/12/2013](#)

MOX	Mixed OXide
NPSH	Net Positive Suction Head
PHX	Primary Heat Exchanger
PP	Primary Pump
SA	Sub-Assembly
SR	Safety Rod
TIB	Total Instantaneous Blockage
UBA	Unprotected Blockage Accident
ULOF	Unprotected Loss Of Flow
UTOP	Unprotected Transient of Over Power
VF	Volume Fraction

[SEARCH]

Deliverable 5.3 – [Two-phase CFD model of the MYRRHA-FASTEF primary coolant loop including all relevant thermal aspects](#)

Dissemination level: [PU](#)

Date of issue of this report: [04/12/2013](#)

1. Introduction

With the increase of computational power and the progress in numerical modelling, Computational Fluid Dynamics (CFD) becomes a tool usable in more and more situations. In the framework of the MYRRHA project [1], through a series of initiatives co-funded by the European Commission, CFD has been already extensively used for the dimensioning and the control of several subsystems and of hypothesis of their variants: spallation target [2], primary heat exchanger [4] , decay heat removal system [3] and so on.

The CFD simulations have been usually restricted to relatively small subsystems, while the global system was investigated by use of nodalized system codes such as RELAP [5] and SIMMER [6]. If we make a crude confrontation in terms of degrees of freedom or in number of control volumes, system codes scale typically from 10^3 up to 10^4 , while CFD 3D codes use on a regular basis 10^5 to 10^6 control volumes for basic applications. In this work, we will reach about 10^7 control volumes. The great improvement in precision given by 3D CFD is however dampened when time enters strongly in consideration. For non-stationary configurations, the time step must scale like the inverse of the control volume size. This means that for a given time laps of simulation, the required computational power scales like the fourth power of the inverse of the control volume size. Thus long transients are much more easily investigated using system codes, even if the information obtained is not very detailed in space.

Unlike time resolution, space resolution can be parallelized and 3D codes strongly use this feature. To fix the ideas, the entice primary loop of MYRRHA (with some necessary simplification) can be modelled with 10^7 control volumes using a base size of 7.2 cm and some refined region at half the base size. Running the simulation with a time step of 0.01 second on a cluster of 256 cores (the maximum we could temporarily afford) allows to compute about 25 s of physical time by day. A lighter model, without the structural part and only 6E7 control volume could simulate 10s of physical time per day on 20 cores of a (more recent) shared memory parallel machine. With these numbers in mind, we can infer that 3D CFD MYRRHA transient simulations are affordable for events lasting no more than a few minutes.

The final objective of this work inside the SEARCH project is to understand the characteristics of fuel dispersion in case of incident leading to the loss of integrity of one or more fuel pin, labelled as Core Disruptive Accident (CDA). By this, we mean investigate if and where the dispersed fuel products will settle and accumulate depending on their size, specific weight and porosity. To reach this objective, we must first construct a full 3D CFD model of the primary system of MYRRHA. We must then make the model reach its nominal condition to be in condition to start the incidental initial event leading to the pin failure.

This document reports on the elaboration of these prerequisite elements. Several CFD models, with increasing levels of precision/complexity have been built, initially based on the revision 1.2 of the MYRHA design [7] then based on version 1.4 of the design [8]. Two additional files have been furnished by the project leader SCK•CEN as reference documents [12]: the first one is a parasolid CAD file containing the reference MYRRHA geometry with some simplification in view of a use for numerical simulation; the second file is an excel worksheet containing the necessary data to build the numerical setup, from physical properties to nominal conditions and under-resolved parts integral parameters (such as pressure drops). Throughout this document, we have made a systematic and intensive use of these two source, without explicit reference. In the meantime, the software starccm+ from CD-Adapco [1] <http://myrrha.sckcen.be>

[SEARCH]

Deliverable 5.3 – Two-phase CFD model of the MYRRHA-FASTEF primary coolant loop including all relevant thermal aspects

Dissemination level: PU

Date of issue of this report: 04/12/2013

8/50

- [2] F.Bianchi et al., Thermo-hydraulic analysis of the windowless target system, Nuclear Engineering and Design, Volume 238, Number 8, page 2135--2145 - august 2008.
- [3] V. Moreau et al., A case history of cfd support to accelerator driven system plant design, Proceedings of The 17th Int. Conf. On Nucl. Eng num. 75588 ASME – 2009.
- [4] V. Moreau, FASTEF Heat exchanger tube rupture CFD simulation, Nuclear Engineering and Design Elsevier pages 42-51 vol. 252 - 2012 doi: <http://dx.doi.org/10.1016/j.nucengdes.2012.06.030>
- [5]<http://www.inl.gov/relap5/>
- [6] <http://www.jaea.go.jp/jnc/zooarai/ejooarai/simmer/>
- [7] MYRRHA Team, “MYRRHA Technical Description Rev. 1.2”, <http://search.sckcen.be/>, February 2012.
- [8] MYRRHA Team, “MYRRHA Technical Description Rev. 1.4”, <http://search.sckcen.be/>, June 2012.
- [9] N. Forgone et al. Operability of the SIMMER-III and SIMMER-IV models for the MYRRHA-FASTEF reactor, SEARCH contractual deliverable D5.1 (Contract Number: 295736),12/2012.

[10], which has been used for all the simulations presented here, has evolved from version 7.02 to version 7.04, version 7.06 and version 8.02. The first MYRRHA CFD models being already obsolete are not reported here. Only the last two models are discussed, the first one using version 7.06 contemplates only the main fluid circulation pattern, omitting the structural part and also omitting a fluid volume around the core raised disconnected from the main one due to the withdrawal of secondary flow bypass. These flow bypass have been withdrawn both to simplify the model and because they were not yet well defined in the design revision 1.4. The second model, run with starccm+ version 8.02, includes the solid part and the dead volume, taking into account the conjugate heat transfer.

A precise description of MYRRHA components, their purpose and their constraints has been performed in the design documents [7][8]. It has been extensively reviewed in a simulation optic in the first deliverable of this work package [9] and will not be repeated here. In the following, we will first concentrate on the CFD geometrical representation of the MYRRHA components at the CAD level, explaining when necessary the simplifications we have chosen, or we have been constrained, to perform. This part is quite detailed to allow cross checking and also to have this document useful for self-checking and reference. Second, we describe the conceptual splitting of the fluid part of the primary system, leading to a division in several fluid regions having their own specificity, either for the geometry or for the required physical setting, mainly specific body forces and heat sources. Third, we give the physical properties of the material simulated, LBE, cover gas, and steel. We then explain extensively how we have coped with all the specific heat sources: core, heat exchanger, external vessel and the specific body forces: core resistance, heat exchanger resistance and pump thrust. We dedicate a specific part to explain how we dealt with the free surface specificity of these simulations.

After having described the numerical setting, we show the result of a simulation with only the fluid part, reaching essentially the nominal flow condition and approaching the thermal stationary condition. A successive 2 minutes transient is analysed to check the flow stability. Last, we present the results relative to the full model, including the structures. The simulation has been monitored for 300 seconds. The monitoring is presented and commented. The thermal time scale of secondary patterns is too large to get a fully statistically converged thermal field. Trends are however clearly identified. The flow stability is furthermore investigated.

[SEARCH]

2. List of 3D-CAD models with geometrical description

The geometry is entirely re-built from scratch inside the starccm+ framework. The geometry is split into some 3D-CAD models. The outcomes of the 3D-CAD models are parts (3D volumes) that can be assembled with further simple Boolean and geometrical transformation and successively transformed into computational Regions. The available operations are more articulated inside a 3D-CAD model than outside of it. Only inside a 3D-CAD model, can the operations be parameterised. Furthermore, the sequence of all operations is automatically updated. This later feature is very convenient but becomes cumbersome when the number of chained operations becomes high, also considering that the tree of chained operation is linear. An access to an operation at the beginning of the tree requires to roll back all the successive operations and unroll them all when closing the access, requiring an increasing time with the increase of the tree length. This is unpractical if one has to work back on parts of the geometry at the beginning of the tree. To avoid excessively long trees, it becomes useful to split the geometry construction in a few distinct parts, the 3D-CAD models. Unfortunately, the part assembled (with Boolean operations) from different 3D-CAD models do not inherit of the updating property.

Currently we have used 6 different 3D-CAD models with self-explaining names.

1. Butterfly
2. Core Barrel
3. Core IPS and SR layout
4. IVFS
5. Porous and voids
6. Main Structure

They are described below together with the parts they produce.

2.1 Butterfly

The Butterfly, aka the Baffle, is a thin vertical shell located in the lower plenum. Its function is to forbid any lost FA to go out of range of the fuel handling machine. The CAD representation, conform to the design specification, is shown on **Figure 1**.

It is foreseen with a huge number of drilled holes, 42 of them at the top and 774 of them in 9 horizontal rows of 86 elements in the lower part.

The first series of 42 holes is geometrically represented in the numerical geometry, however with squared holes of equal cross section, less demanding in mesh term for a reasonable description.

It has been suggested to simulated the remaining 774 holes by mean of a porous media, with a porosity about 0.9 in the lower 1.48 m section. After analysis, this suggestion does not seem really suited for this case. In effect, the flow passing through the drilled shell is strongly orthogonalised with respect to the shell. This can be obtained with a porous media by setting a very high tangential resistance coefficient with respect to the normal coefficient. However, the shape of the butterfly does not allow a simple specification of the normal direction. Moreover, a porous media approach is adequate when the underlying basic structure has a very small size in confront with the resolved scale. We can infer that the flow is artificially distorted on a range of ten times the small structure size. In the current configuration, the elementary structure is more than 20 cm large, leading to an inadequate flow in almost all the inside of the butterfly.

[SEARCH]

We have followed an alternative strategy consisting in merging several holes together to make larger (square) holes, still reasonably covering the shell bottom part. In this way, at least the orthogonalisation of the flow is enforced. The result is displayed in **Figure 2**.

As the strategy to be used may change in the future because of a renewed interest or thanks to more available computational power, a specific region around the butterfly is generated separately. The width of the region at the top is smaller than at the bottom because of the nearby presence of other structures: the Core Barrel and the IVFS.

Three parts are generated: (i) the solid Butterfly, (ii) the fluid region around it and (iii) their union.

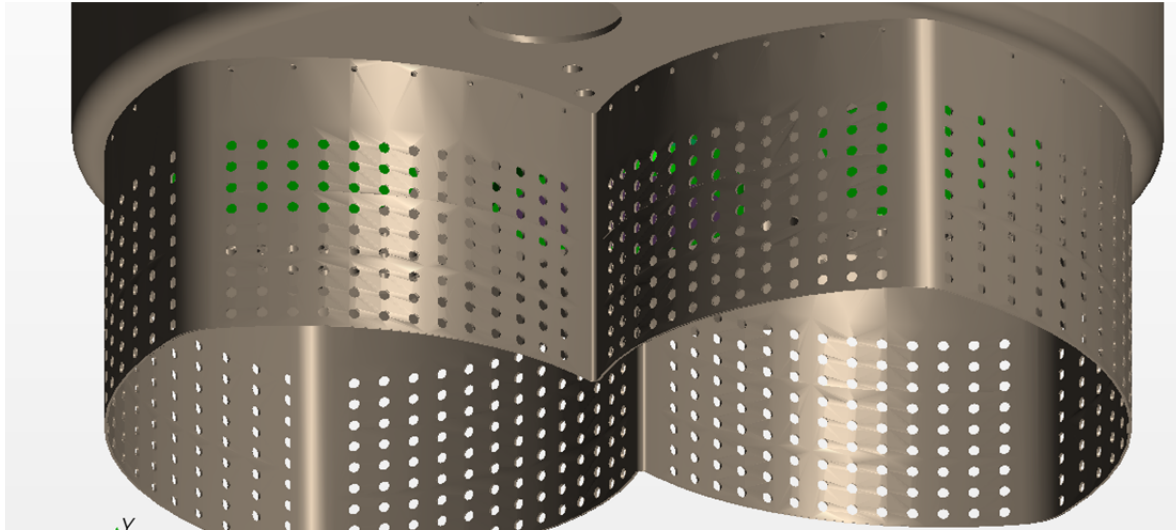


Figure 1: CAD representation of the butterfly, conform to the design.

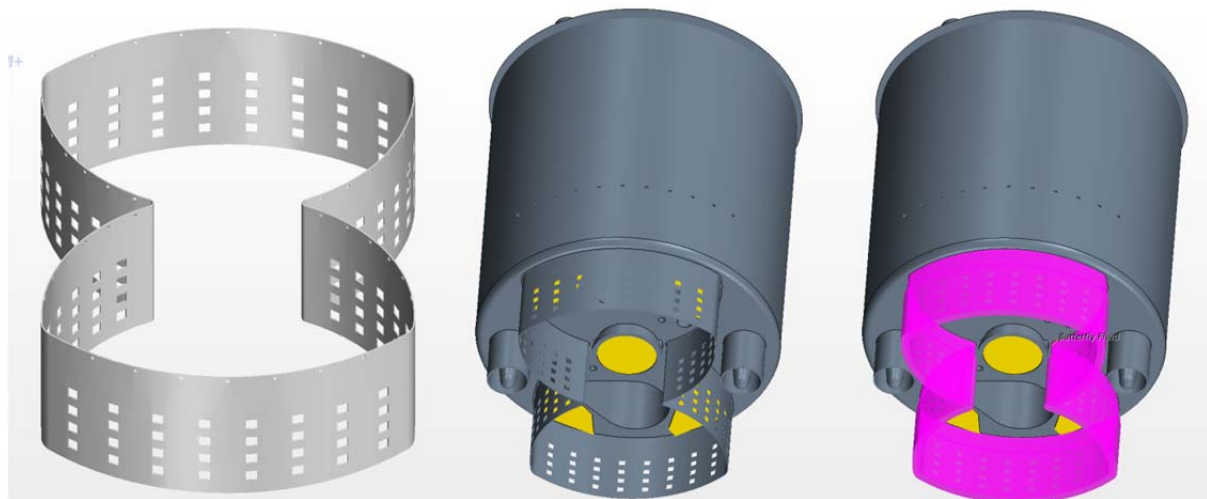


Figure 2: CFD Geometrical model. Left, Butterfly Part. Centre: view on the diaphragm from below. Right, Fluid Butterfly region highlighted.

2.2 Core Barrel

The core barrel envelop is a simple structure that can be generated by revolving a 2D sketch. It is however drilled with an array of staggered circular holes in its upper part. The generation of the holes may interfere with other parts, like the Porous ACS and the IPS/SR guide tubes, making its separate construction convenient.

[SEARCH]

The numerical geometry is conform to the model design, except that it has been cut over quote $y=4.4$ m, as the upper part, filled with gas is of no real current interest. Only one part is generated: the solid Core Barrel, as shown in **Figure 3**.

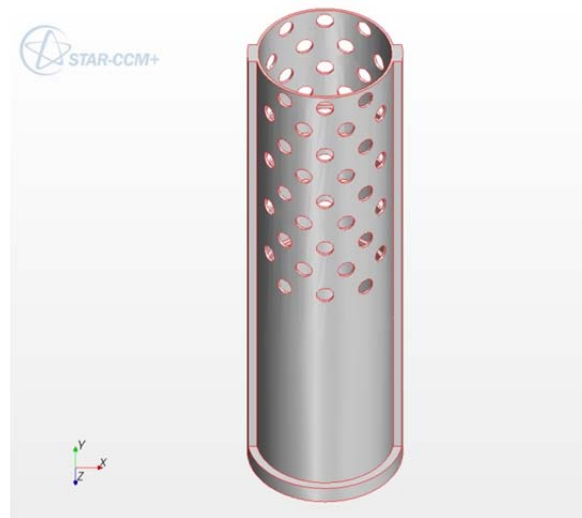


Figure 3: core barrel part in CFD geometry

2.3 Core, IPS and SR layout

The numerical approximation of the core is a quite delicate matter. Suggestion has been given to have a concentric cylindrical structure, each layer corresponding to a specific type of position. This approximation is good for axial-symmetrical 2D codes such as SIMMER. While also acceptable for a 3D code, we think that the available computer resources allows to improve further the level of description, describing roughly but separately all 151 core positions. However, it is unrealistic to manipulate separately each of the positions and some kind of factorisation must be performed.

Thus, the Core has been split in three main functional fluid parts:

1. The FAs: for 69 positions
2. The Inner Dummies with the CR: for $24+6=30$ positions
3. The Outer Dummies: for 42 positions,

The IPS (including the Target slot) and SR positions will be removed in a successive step and so can be treated together with the FA positions at this stage.

Each part is composed of an array of pipes (one pipe per position) connected through an upper and a lower thin horizontal layer. Each horizontal layers is connected and separated from the others, while their union completely fills a cylindrical lab above and under the core. Such a decomposition of the horizontal layer is possible only if we perform some preliminary simplification.

Each position has a dedicated space, but not all the space in the position is occupied by the fluid. Moreover, only the top cross section occupied by the fluid has importance as it controls the fluid outlet kinetic energy (for a given mass flow rate). As a crude estimate, we have considered that only 49% of a FA position is effectively occupied by the fluid, such that the linear dimension of the corresponding hexagon is 70% of the total available. Each position is therefore represented by an hexagonal fluid rod clearly separated from the others. The distance between the hexagons allows to build a connected route for the top and bottom layer. A side effect of this approach is that we do not need any more to deal with porous media in this region.

[SEARCH]

The Inner Dummies and the CRs are assembled in the same part. This is for topological reasons, otherwise we would have a separate part for each CR. The CRs can be discriminated from the Inner Dummies on a radius basis and a source term can easily be localised on this criterion. This has been foreseen for a heat source in the Inner Dummies in the sub-critical configuration. The target mass flow rate is different for an Inner Dummy and a CR. As the resistance coefficient in the momentum equation can revert a relatively complex form, we choose to keep the same coefficient for both Dummy and CR positions and to cope with the flow difference with a proportional reduction of the CR cross section. We used a 78% linear reduction factor to build the CR rods.

The choice of the penetrations inside the Core Barrel having to be represented is a delicate matter. We have chosen to represent only the obstruction caused by the IPS and by the SR. They are approximated by plain hexagonal rods. There are (6+1) IPS and 3 SR because our reference configuration is the critical one. To reduce the number of generated parts, the 10 hexagonal rods are connected to a thin horizontal plate above the top of the physical domain. The rods are larger than the FA rods and their extrusion down to the core bottom effectively cancel the corresponding positions from the fluid domain.

The core is enclosed in a cylinder. The FA rods have hexagonal shape. The upper layer is 10cm high. The lower layer is 15cm wide. A buffer cylindrical part is built below the core, 20 cm high.

The last parts built in this 3D-CAD model are two ACS circular horizontal support grids. They are drilled with the IPS and SR guide tubes.

A total of 8 bodies is built here:

- The IPS + SR bundle
- The two ACS grids
- The core bottom
- The FAs assembly
- The Inner Dummy + CR assembly
- The Outer Dummy assembly
- The overall core cylindrical volume.

These bodies are illustrated in **Figure 4** and in **Figure 6**, the reference core structure being shown in **Figure 5**.

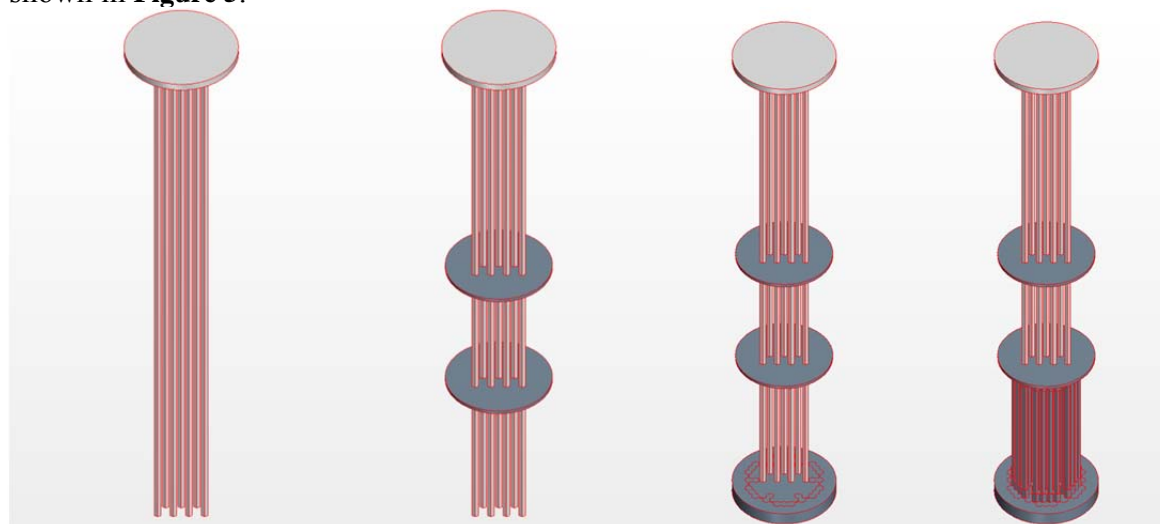


Figure 4: Geometry CFD model. From left to right: 1-IPS+SR bundle, 2- adding ACS grids, 3- adding core bottom, 4- adding FAs.

[SEARCH]

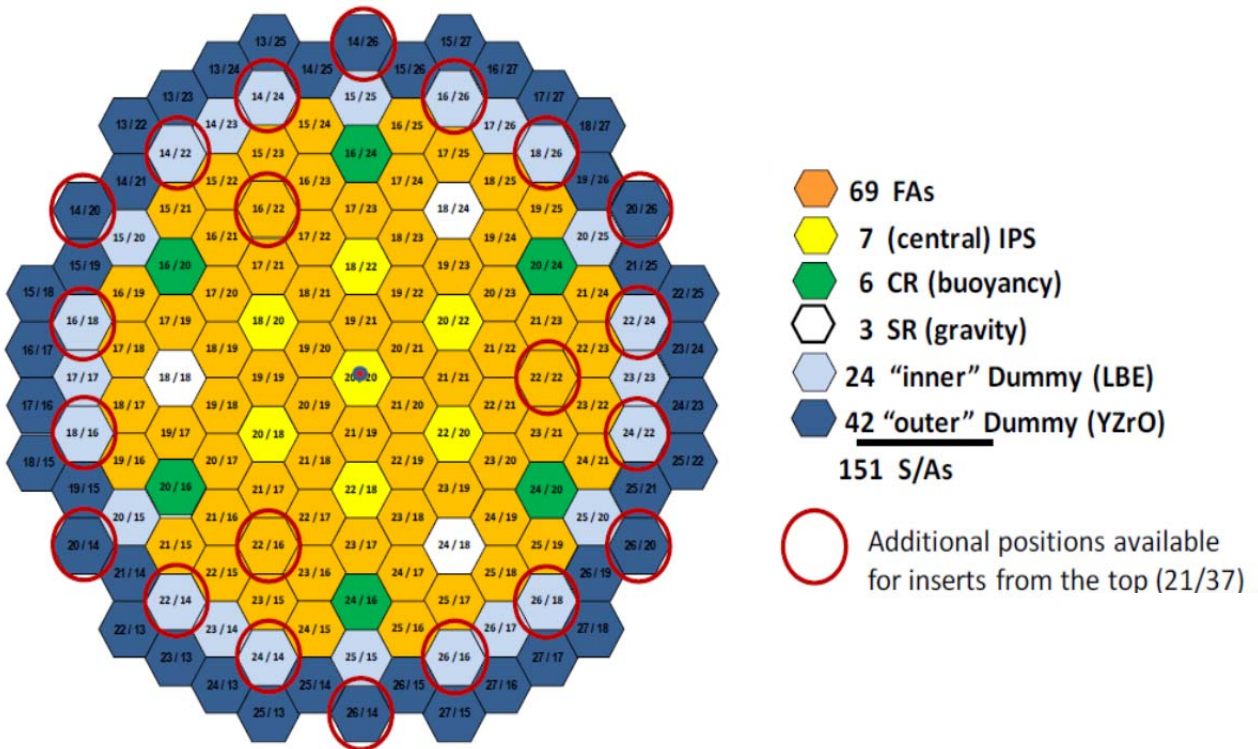


Figure 5: reference core structure

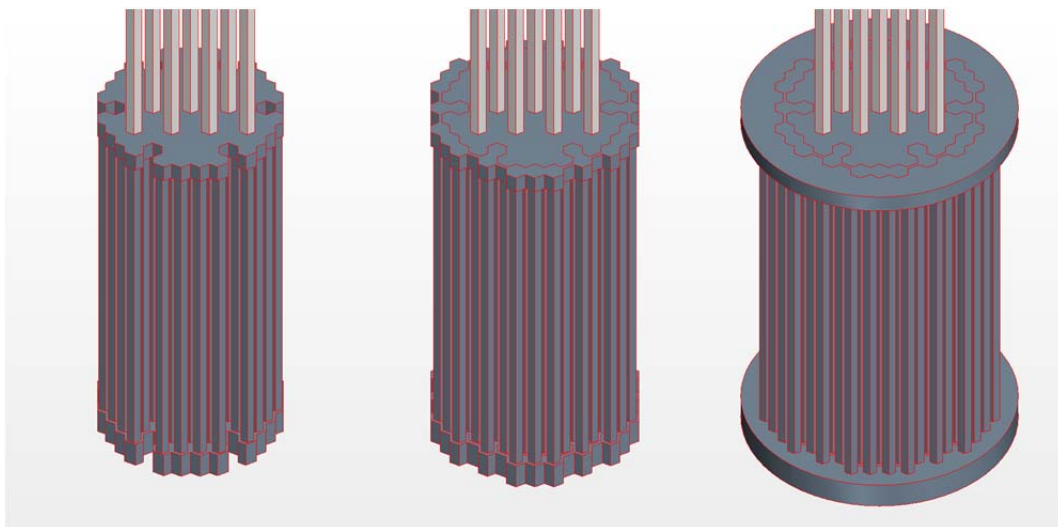


Figure 6: CFD geometry. Left, FA bundle around the IPS+SR bundle. Centre: added Inner Dummies. Right, added Outer Dummies.

2.4 IVFS

The IVFS (In Vessel Fuel Storage) should in principle consist of four series of 69 cylinders in which are located the stored FAs. The four series are divided into two different arrangements. Following the Butterfly methodology, we have reduced the 69 cylinders to 9 larger ones with the cross section equal to 69/9 FAs. In this way the FA resistance coefficient in the

[SEARCH]

Deliverable 5.3 – Two-phase CFD model of the MYRRHA-FASTEF primary coolant loop including all relevant thermal aspects

Dissemination level: PU

Date of issue of this report: 04/12/2013

momentum equation is also valid for the IVFS. The 9 cylinders are located inside the envelop of the former 69 cylinders, see **Figure 7**. They are connected through a thin horizontal layer in the lower plenum, 10 cm high, as illustrated in **Figure 8**.

Because, at the 3D-CAD level, bodies can only consist of connected parts, a total of 8 bodies are produced, one for each of the 4 fluid parts and one for each of the 4 solid parts.

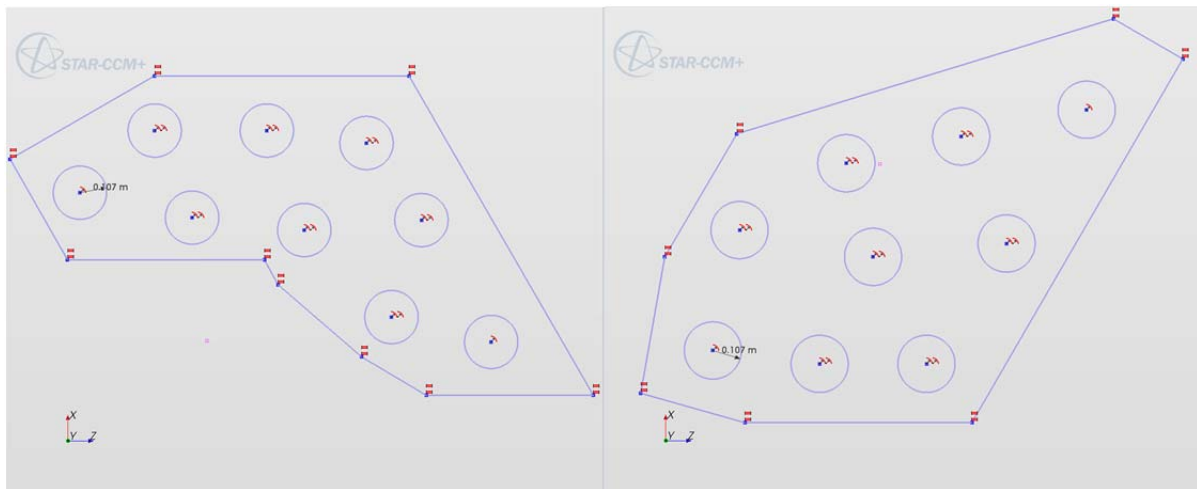


Figure 7: Sketch of the IVFS solid part with holes to host the aggregated FAs.

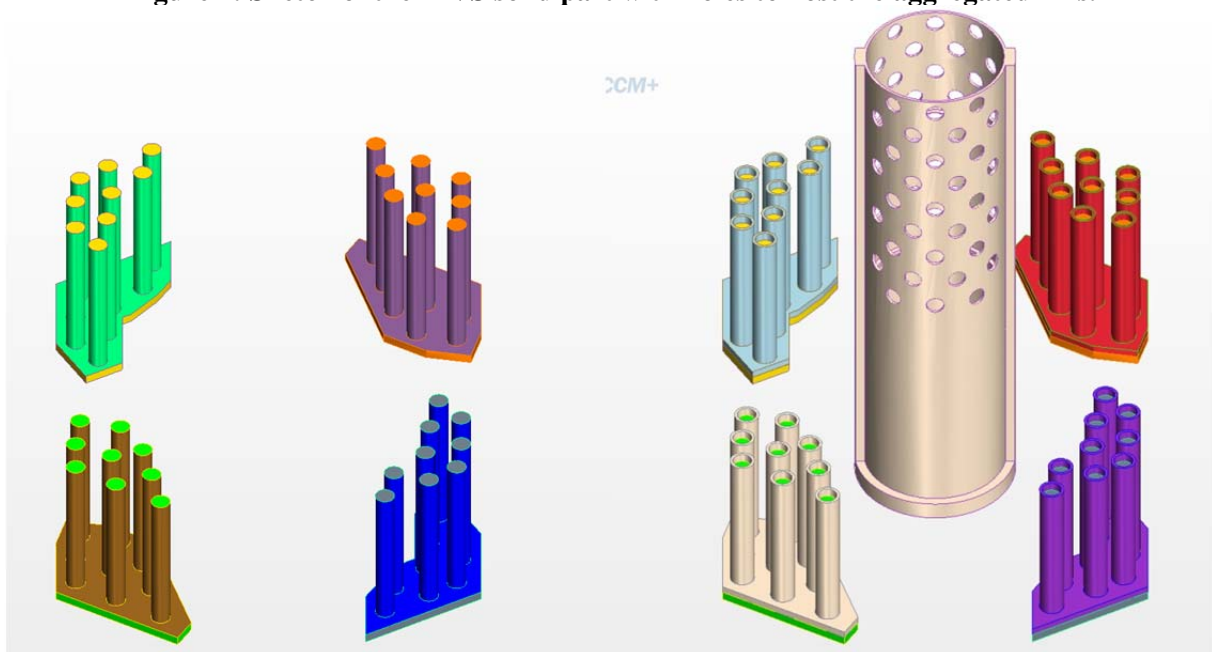


Figure 8: Left, IVFS fluid part. Right, added the IVFS solid part and the core barrel.

2.5 Porous and Voids

In this 3D-CAD model, we have grouped different simply shaped parts. These are:

- The four porous part of the HXs
- The two annuli 20cm high where the PP head is located.
- The two voids corresponding to the volumes occupied by the PP assembly over the Upper Plate.
- The voids corresponding to the volumes occupied by the Silicon doping assembly, connecting to the top. The bottom falls into to the dead volume around the core.

[SEARCH]

These parts are shown on **Figure 9**.

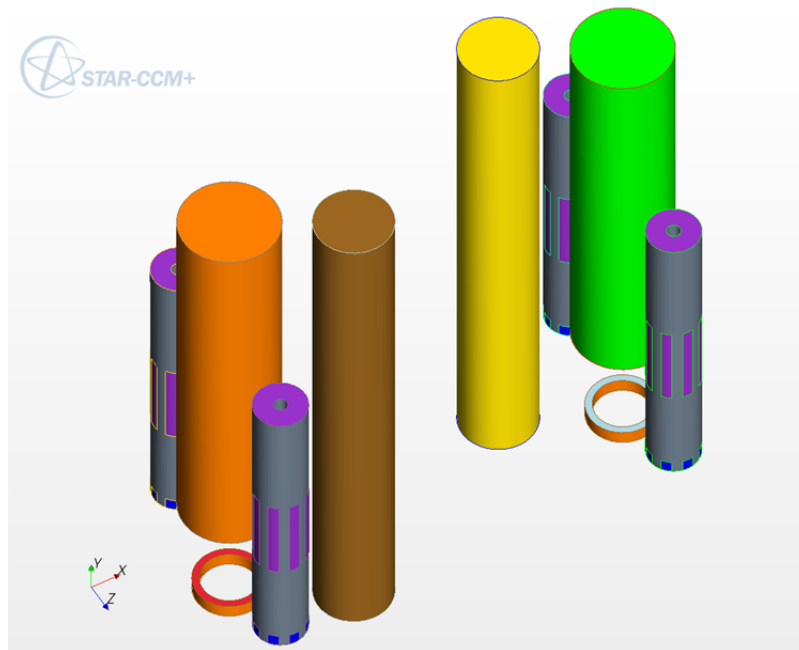


Figure 9: CFD geometry. Active part of the 4 HXs, 2 pump thrust rings, voids for the two Silicon doping slots and the 2 PP upper casing.

2.6 Main Structure

Last but not least, the Main Structure 3D-CAD model contains essentially the structural parts which will be either simulated as solid or simply subtracted to the main fluid volume. The main components are listed hereafter and then more extensively described.

- Base fluid: fluid volume obtained by fully filling up the external Vessel.
- Vessel: the fluid container. Cylindrical with a tori-spherical bottom.
- HX1, HX2, HX3, HX4: the solid part, except the tube bundle, of the HXs.
- PP1, PP2: the solid part of the PP assemblies below the Upper Plate.
- Fluid Numerical Top: located above the physical domain. Name self-explanatory.
- Base solid: comprise the Inner Vessel, the lower plate, the upper plate, the vertical penetrations, the inter plate shells and the IVFH penetrations.

2.6.1 Reactor Vessel

The CFD part is shown on **Figure 10**. The fluid domain is enclosed inside the reactor vessel up to quote $y=6.71\text{m}$. When the structural part is not part of the simulation, the reactor vessel internal boundary is the CFD domain wall boundary, and is treated as adiabatic. If the structure is contemplated, the external part of the vessel in the simulation domain boundary and will exchange heat to the un-simulated surrounding by radiative transfer.

[SEARCH]

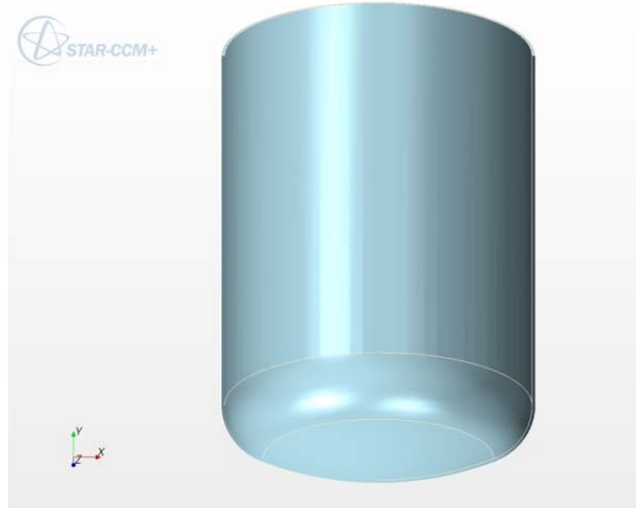


Figure 10: CFD Geometry. Vessel with torispherical head.

2.6.2 Heat exchangers (HXs)

The solid part of the HXs is obtained by revolving a simple sketch. The openings are performed in a second step by two circular pattern cuts.



Figure 11: Volume of a HX solid part.

The CFD model is essentially conform to the simplified model, except for a top cut and the exact shape of the tori-spherical bottom, see **Figure 11**. The HX tube bundle is modelled as a porous medium described later on.

2.6.3 Base Solid (Diaphragm)

The Base Solid is the part of the Diaphragm which essentially separates the hot and the cold plenum. It is a quite articulated structure, see illustration in **Figure 12**, needing to be split in several sub-components:

1. Lower plate
2. Cylindrical shell
3. Upper plate
4. Casing
5. penetrations: for PHX, Fuel Handling, recovery port, LBE inlets, fuel transfer channel and wet-sipping devices.

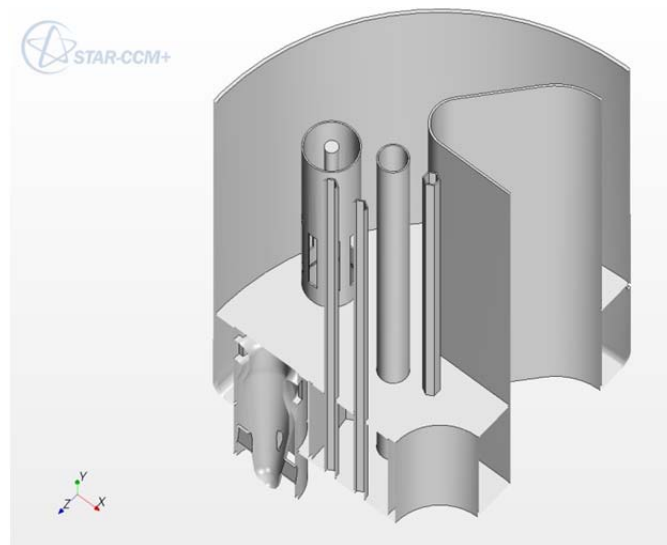


Figure 12: CFD geometrical model. Base Solid.

2.6.3.1 LOWER PLATE

Penetrations:

- Core
- 2 x Fuel Handling
- 2 x PP
- 2 x Fuel Transfer channel
- 6 x various: LBE inlet/outlet, wet sipping.

The penetrations do match exactly the pipes external diameter, not leaving holes for flow bypass. Geometry is shown in **Figure 13**.

[SEARCH]

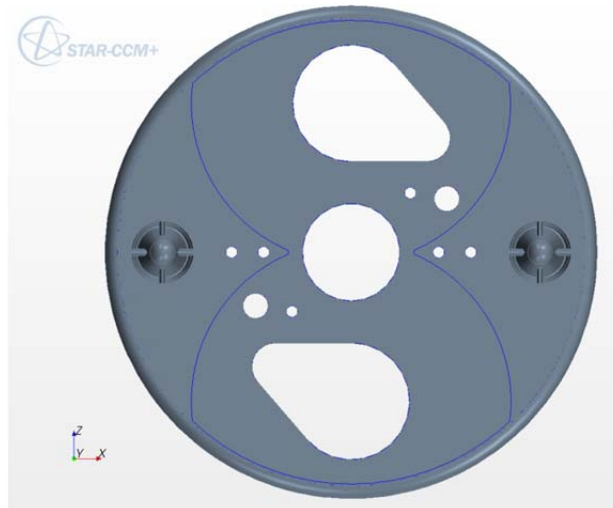


Figure 13: CFD geometry. Lower plate part with pumps inserted.

2.6.3.2 CYLINDRICAL SHELL (INNER VESSEL DIAPHRAGM)

Connects the lower plate to the top.

Vertical part cut 21 cm below the top so as to maintain communication with the cover gas plenum.

The circular holes near the top are eliminated from the CFD simplified model.

Also 2 series of 11 circular holes near the bottom for recovery of storage FAs recirculation.

They have been transformed in hexagonal shape of equal cross section, see **Figure 14**.

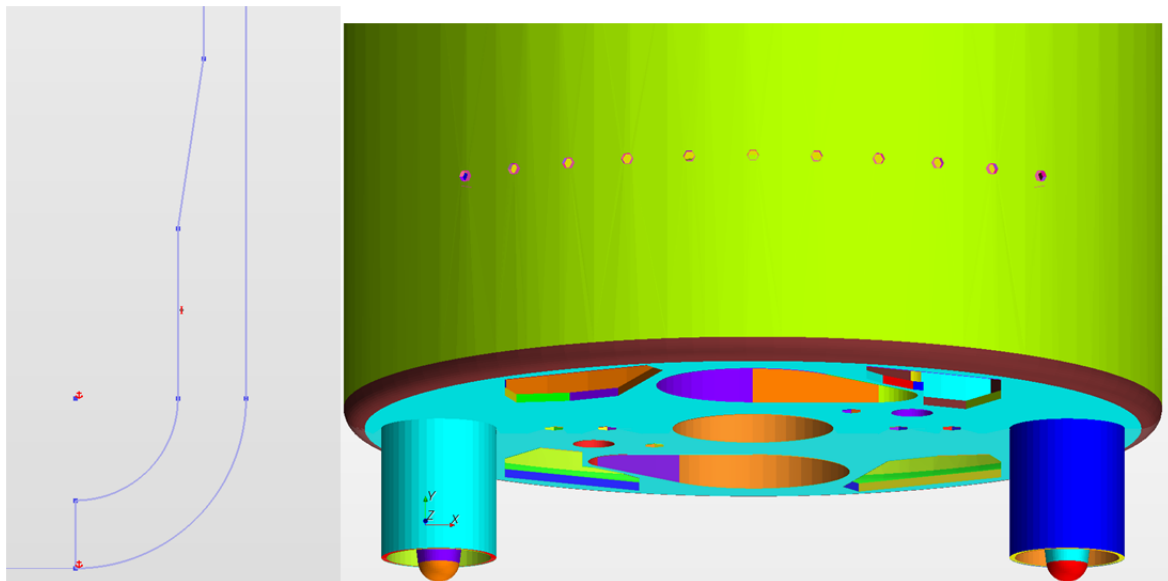


Figure 14. Left: Diaphragm sketch. Right: Holes location.

2.6.3.3 UPPER PLATE

The upper plate sketch is shown on **Figure 15**. Its construction characteristics are given below.
Penetrations:

- Core.
- 2 x Fuel Handling.
- 2 x Si doping.

[SEARCH]

- 4 x PHX.
- 2 x Fuel Transfer channel.
- 6 x various: LBE inlet/outlet, wet sipping.

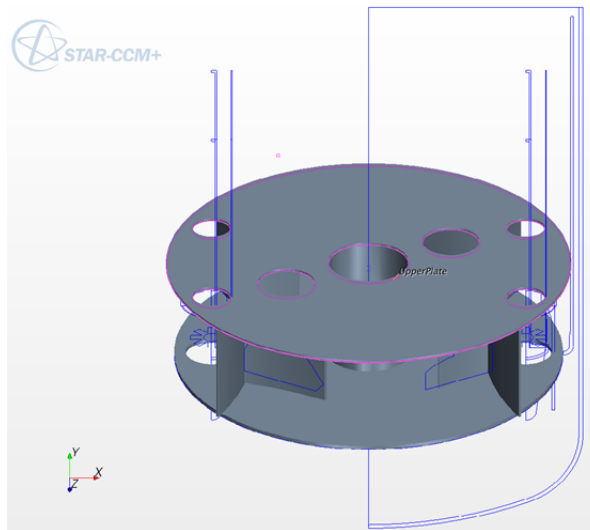


Figure 15: CFD Geometry. Upper Plate during building stage (other cuts afterward).

2.6.3.4 CASING

The casing, shown in **Figure 16**, separates the volume between the lower and upper plates in three conceptual (5 separated) parts.

1. the core surrounding volume.
2. The PP/PHX assemblies (2).
3. The fuel repository assemblies (2).

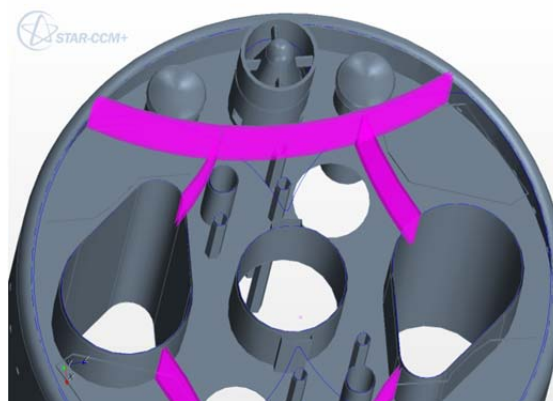


Figure 16: casing view from below.

The CFD model is essentially conform to the simplified model. Deviations should be below the centimetre range. It is built on arcs of circle: $C1x=7.56m$, $C1z=0m$, $Ri1=5.3m$, $C2x=C2z=3.5m$, $Ri2=2.95m$, $C3x=4m$, $C3z=-7m$, $Ri3=5.98m$.

[SEARCH]

2.6.3.5 PENETRATIONS

There are various tubular penetrations connecting the cover gas region to the lower plenum through the upper plate and the lower plates. These are for:

- Fuel Handling and
- Small penetrations: LBE inlets-outlets, fuel transfer channel and wet-sipping devices.

All the penetrations are cut in the CFD model 21 cm below the top to let room for communication with the cover gas plenum. They are illustrated in **Figure 18**.

2.6.3.5.1 IVFHM (IN VESSEL FUEL HANDLING MACHINE)

The penetration shape is obtained by connecting two arcs of circle by common tangents. The IVFHM in itself is a complex unknown machine not represented at the CFD level. Its view from below is given in **Figure 17**. Only its envelop penetration is represented.

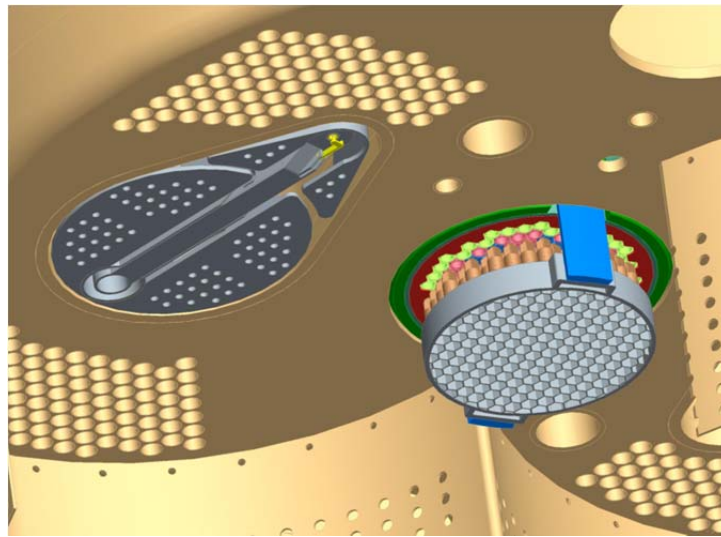


Figure 17: View from below of the lower plate. Design rev. 1.4. Position and orientation of the Fuel Handling penetration .

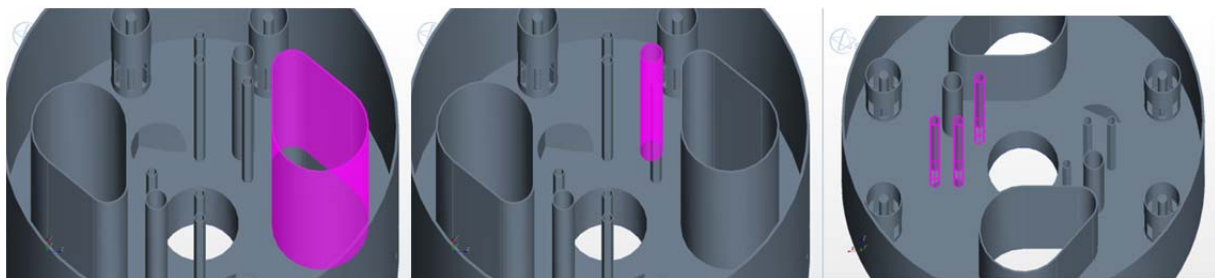


Figure 18: Left: IVFHM. Centre: Fuel transfer Channels. Right: LBE inlet-outlet and wet sipping device.

2.6.3.5.2 SMALL PENETRATIONS

The Fuel Transfer Channels are large enough to be correctly represented as circular tubes, while the other penetrations (which are smaller) have their geometry approximated by a hexagonal tube with the same internal cross section. This is to keep a better control for the CFD mesh discretization at the foreseen base mesh size.

[SEARCH]

2.7 Numerical Top

A Numeric top has been added to the computational domain to cope with the mass/volume constraint of the CFD model. Its top is a Stagnation Pressure Inlet boundary, and a volume fraction sink term is set inside its volume so as to ensure that a real inlet condition is met. Its size and location, as shown on **Figure 19**, is based on the “rule of thumb”.

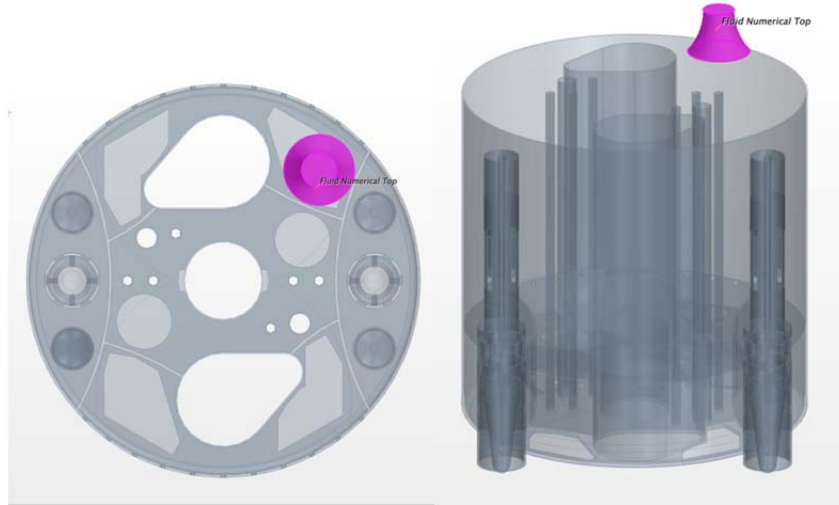


Figure 19: Position of the numerical top volume in the CFD geometry.

2.8 Primary pumps

2.8.1 Pump chimney

The PP chimney is modelled as a void as described in the “porous and Void” section.

2.8.2 Pump guide lower part

It extends down to the diaphragm lower plate. There are 6 rectangular evenly spaced openings. The central profiled body of the pump is made of three parts.

- A top convergent guide, bringing the lateral incoming flow into a vertical flow.
- A straight vertical part where the propeller blades are hosted.
- A conical divergent.

[SEARCH]

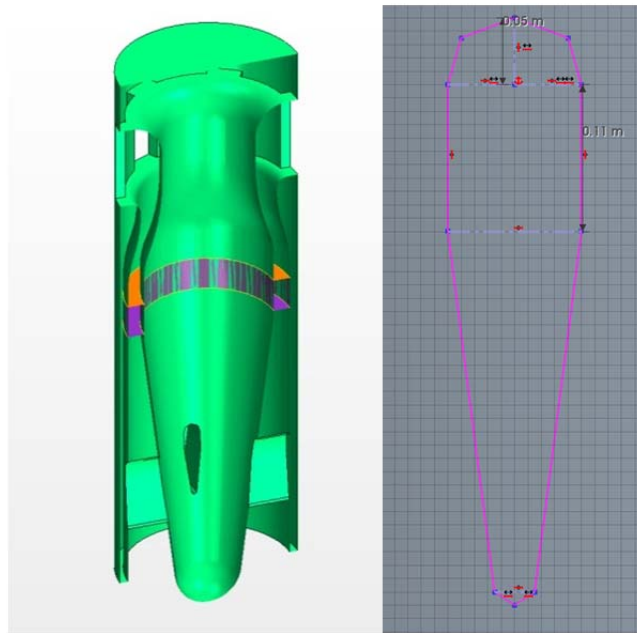


Figure 20: Left, PP part with thrust region. Right, PP winglet sketch.

Four vertical winglets connect the conical divergent to the pump guide and serve to damp the swirling motion in outlet. They are very thin with regards to the mesh size so they are approximated with a piecewise linear perimeter as shown on **Figure 20**, right. The CFD representation of the pump guide completed with the winglets is shown on **Figure 20**, left.

3. CFD Fluid regions

The fluid part of the computational domain is divided into several regions, not necessarily connected, which differ at least in one way in their numerical treatment. The list of CFD fluid domain is given below:

1. Barrel Envelop: region around the core barrel and over the core, requiring a finer mesh definition.
2. Butterfly Fluid: region around the solid Butterfly, requiring a finer mesh definition.
3. Core Bottom: small cylindrical region below the core constrained laterally by the Barrel, which may require a specific mesh size and serves as interface between the core regions and the main fluid region.
4. Core FAs (Fuel Assemblies): array of fuel assemblies connected together at top and bottom by an horizontal layer. Requires a specific heat source and momentum resistance force.
5. Core Inner Dummy: array of Inner FA dummies and CR connected together at top and bottom by an horizontal layer. Requires the same force as the Core FAs, but no heat source in critical configuration. The CR have a smaller section to account for the different foreseen mass flow rate. In under-critical configuration, the heat source in the added FAs is easily differentiated from the CR by a simple geometrical criterion (the radius).
6. Core Outer Dummy: array of Outer FA dummies connected together at top and bottom by an horizontal layer. Requires a different force as the Core FAs, and no (or very small) heat source.
7. Fluid IVFS (In Vessel Fuel Storage): four series of cylinders with the same resistance as in the FAs and a different heat source to represent the fresh replacement cores and the burned ones. The cylinders are connected through a thin horizontal layer in the lower plenum.

[SEARCH]

8. Fluid Main: all fluid parts that remain to be modelled. Divided into two unconnected parts, a small one trapped between the Core and the Porous ACS (this part is given a specific region in the least CFD model), the other one, the large one, comprising the lower and the upper plenum connected through the top gas region.
9. Fluid Numerical Top: small part at the top of the computational domain with a stagnation inlet and a VF sink (together with the related heat sink). It is added in order to easily comply with the volume and mass conservation constraints.
10. Fluid PP Thrust (Primary Pumps): two horizontal annuli 20cm high where the pumps deliver their head (fitted to get the nominal mass flow rate). This region separates the PPHX assemblies from the lower plenum.
11. Porous ACS (Above Core Structure): two horizontal grids inside the Barrel to fix the various guide tubes. It is treated as a slightly resistive porous material.
12. Porous HXs (Heat eXchangers): the active part of the HXs separating the upper plenum from the PPHX assemblies. It is treated as a porous medium to take into account the secondary coolant (water) tube bundles. Requires a specific porous description and heat source (sink).
13. PPHXs (Primary Pump - Heat eXchanger Assemblies): the two parts region between the HXs and the PPs. May require a specific mesh size.

The regions labelled Main and PPHXs are obtained by subtraction of all the solid structures, of all the other fluid regions and of all the a priori known dead volumes from the volume given by the Outer Vessel envelop. This subtraction gives also an isolated dead volume around the core and a complementary volume inside the core around the FAs. Both volumes are discarded when the structural part is not contemplated. When the structural part is considered, the volume inside the core around the 151 positions is treated as steel while the dead volume around the core is simulated as a fictitious solid LBE.

4. Physical properties

For the LBE, the physical properties are directly taken from the LBE handbook [11] and reported here for commodity.

Parameter (symbol)[units]	Formula (temperature in K)	Value at 300 C	Value at 350 C	Value at 400 C
Molecular Weight [kg/kmol]	207.2			
Melting Point [K;C]	397.7 124.5			
Density[kg/m ³]	11096 – 1.3236 T	10337.4	10271.2	10205.0
Dynamic viscosity (μ) [kg/m/s]	$0.494 \cdot 10^{-3} \exp(754.1/T)$ approximate polynomial form $10^{-5} \cdot [605 - 1.078 T + 0.0006 T^2]$	$1.84 \cdot 10^{-3}$	$1.66 \cdot 10^{-3}$	$1.51 \cdot 10^{-3}$

[SEARCH]

Thermal conductivity (k) [W/m/K]	$3.61 + 1.517E-2 T - 1.741E-6 T^2$	11.73	12.28	13.03
Specific heat (C_p) [J/kg/K]	$159 - 2.72E-2 T + 7.12E-6 T^2$	145.7	144.8	143.9

Table 1: LBE physical properties

Most of the structure, and seemingly all the resolved structure parts are made of AISI 316L steel. The FA wrappers and the core support plate are made of T91. However, these component are geometrically poorly resolved.

In practice, the structure is considered of only one material: AISI 316L. From the Atlas technical handbook [13], we find:

- **Density:** 8000 kg/m³
- **Thermal conductivity:** 16.3 W/K/m at 100C and 21.5 W/K/m at 500C (thus linear interpolation $k=11.45 + 0.013 T$)
- **Heat capacity (C_p):** 500 J/K/kg

5. Momentum and Heat Sources

5.1 Core

The core is described on a slot/position basis. All slots are hexagonal with the same cross section except the CR which have a cross section reduced to 60%.

	FA	Inner dummy	CR	Outer dummy	Total
Number	69	24	6	42	141
Flow %	100	100	60	65	
Eff. Number	69	24	3.6	27.3	123.9
Flow/Position [kg/s]	76.2	76.2	45.7	49.5	
Flow [kg/s]	5258	1829	274	2079	9440
Mean velocity [m/s]	1.57	1.57	1.57	1.02	
Bulk Friction factor [adim]	12.82	12.82	12.82	31.0	
Distributed pressure loss [kPa]	164.0	164.0	164.0	167.5	
Boundary friction factor [adim]	0.47	0.47	0.47	0.47	
Boundary pressure loss [kPa]	6.0	6.0	6.0	2.5	
Pressure loss [kPa]	170	170	170	170	

Table 2: Foreseen flow, velocity and pressure losses through the core components.

5.1.1 Hydraulic resistance (as a force density)

The foreseen mass flow rate , velocity and pressure losses through the core components are given in Table 2. The rationale to get these numbers are given below.

We take the resistance density R in the form: $R=-0.5\epsilon\rho v^2$, distributed over 1m height, such that the effect is a total pressure loss $dP=1.7$ Bar. Inlet and outlet pressure drop should

[SEARCH]

naturally be included in the CFD simulation and not accounted for twice. We must evaluate them so as to get the correct total pressure loss.

The inlet is assimilated to a sudden contraction and the outlet to a sudden expansion. The expansion coefficient used is $\beta=0.49$. The friction factor is: $\varepsilon=0.45(1-\beta)+(1-\beta)^2=0.47$, the velocity being always the velocity inside the hexagonal slots.

The total foreseen mass flow rate is $m=9440$ kg/s. The mean density taken is $\rho=10377$ kg/m³.

5.1.2 Core Heat source

The heat source is distributed over 60 cm height across the centre height and restricted to the FAs. The heat source follows a parabolic profile in the radial direction in the form:

$$H=a[h_0-(h_0-h_1)(R/R_1)^2]=3.57e8(2.15-5.25R^2),$$

The parameter a is fitted to get a total of 100 MW from a direct measure in the Starccm+ model.

We take $h_0=2.15$, $h_1=1$ and $R_1=46.8$ cm. To get a distribution close to the one given in Figure 22. With these parameters, it comes $a=3.57E8$.

The heat source distribution is shown in **Figure 21**.

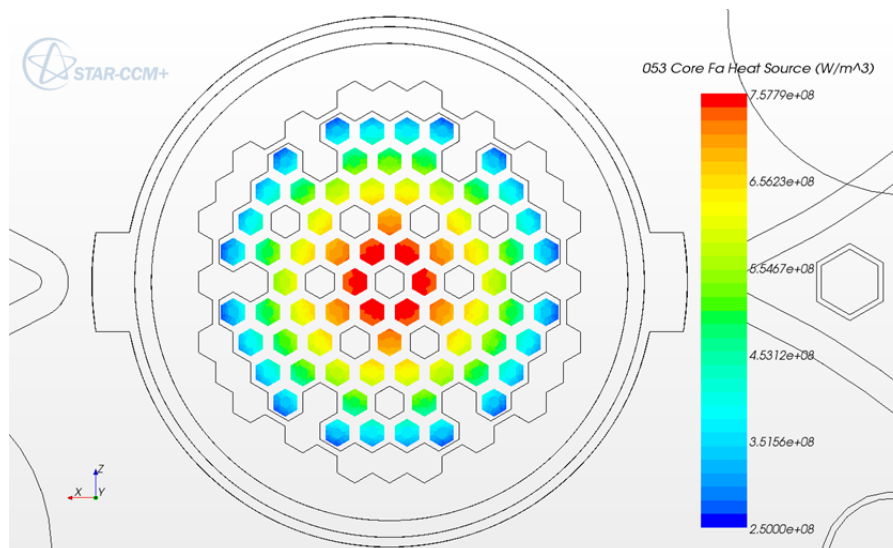


Figure 21: Heat source for a 100 MW critical core.

[SEARCH]

Deliverable 5.3 – [Two-phase CFD model of the MYRRHA-FASTEF primary coolant loop including all relevant thermal aspects](#)

Dissemination level: PU

Date of issue of this report: [04/12/2013](#)

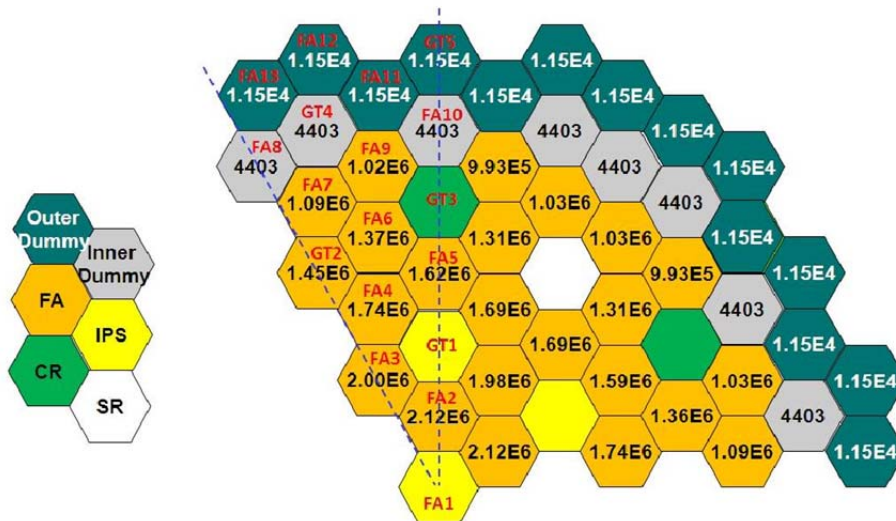


Figure 28 – Radial power distribution in MYRRHA reactor core (Ref. [4])

Figure 22: Foreseen radial power distribution for a 100 MW critical core.

5.2 PHX

The relevant characteristics of the group of the 4 PHXs are:

- Effective superficial cross section: S
- Nominal flow rate: $M=9440\text{kg/s}$.
- Mean LBE density: $\rho=10334\text{ kg/s}$.
- Mean superficial nominal velocity: v .
- Active length: L .
- Characteristic residence time: τ .
- Tubes external diameter: d .
- Number of tubes: N .
- Cross section taken by the tubes: $S_t= N \pi d^2/4$.
- Porosity: $\text{Por}=1-S_t/S$.
- Real cross section: $S_r=S-S_t$.
- Mean real vertical nominal velocity: $u=v/\text{Por}$.

5.2.1 PHX Heat source

The heat source must bring the hot flow from 350 C to 270 C in a characteristic time τ . This is a conservative assumption for a total heat source in the system of 110 MW. The core power is only 100 MW and the power in the IVFS is taken to 2 MW. With a diffuse heat release essentially from Polonium decay about 0.5 MW, the total heat source amounts to 102.5 MW. As we constantly try to keep the cold plenum to 270 C, we expect a mean flow temperature of 344 C at the PHX inlet. This is however true only for extremely large times. In effect, the decay heat power in the IVFS slowly heats the passing LBE which goes afterward to the cold plenum top lateral annulus and does not participate for a long time to the temperature of the main flow. The expected temperature at the PHX inlet is therefore about 342 C for a quite long intermediary asymptotic time.

[SEARCH]

The heat source is distributed over the entire porous part (representing the surrounding of the tube bundles) of the PHXs. We take the heat source under the form:

$$h_s = -\rho C_p(T-T_0)/t,$$

with adjustable parameter t . This parameter is adjusted during the thermal transient of the simulation so as to keep the PHX outlet flux mean temperature at 270 C, this last temperature being monitored.

The cold shut down as well as the water inlet temperature at the PHX secondary side is 200 C, while the mean water size wall Temperature is 221 C. There are slow flow regions, on top and at the bottom near the central water tube feeder, in which the wall temperature is inadequate. The heat sink formula is therefore quite approximate and we choose $T_0=210C$.

5.2.2 PHX Hydraulic resistance

The hydraulic resistance is split into two contributions, the vertical one, along the y axis, and the horizontal one (radial). It is given under the form of a distributed force f such that

$$f = -(A+B|v|)v,$$

with A and B two diagonal tensors.

The vertical coefficient are using the following parameters:

- Mean dynamic viscosity: $\mu=1.80e-3$ Pas/m
- Wetted perimeter: Pe
- Hydraulic diameter: d_h
- Vertical Reynolds Number: $Re = \rho u d_h/m$.
- Fanning friction factor: $f_f = 0.046 Re^{-0.2}$.
- Estimated effective length: L
- Vertical pressure loss: $\Delta P = 2\rho f_f u^2 L/d_h$

The next step is to state that: $(A_y+B_y|v|)v = \Delta P/L$.

We also force that $B_y|v|=100 A_y$ for v the mean superficial velocity under nominal condition.

This is to ensure that the quadratic part is dominant when the flow is turbulent but also that the resistance becomes linear when the flow becomes laminar.

To avoid freezing of the cover gas in contact with the HX top, we have set the parameters proportional to the mixture density.

The transverse friction loss coefficients are based on the formula for cross flow over staggered tube banks:

$$dP = Eu \rho u^2/2.$$

Eu is the Euler number and u is the mean velocity in the smaller cross section. It is related to the mean superficial velocity v by $u = v*a/(a-1)$, where a is the Pitch to diameter ratio. The pressure drop dP is the one across a single tube row, that is for a distance $\delta l = \text{Pitch}*\sqrt{3}/2$.

The problem here is that the Euler number depends slightly on the Reynolds number. It is decreasing from 0.3 to 0.2 when the Reynolds number increase from $1e4$ to $1e5$. There is no however a typical HX cross flow Reynolds Number. So, we set $Eu=0.25$ as a first heuristic guess.

The formula is transformed in starccm+ variables and this pressure loss can be entirely transferred to the quadratic coefficient: $\delta P/\delta l = B_r v^2$, giving:

$$B_r = Eu \rho a^2 / (2 dl (a-1)^2).$$

The radial quadratic coefficient would be more than 50 times the vertical one.

There is a flaw in this approach, because the flow is essentially not transverse and the radial component of the velocity is generally much lower than the vertical one. It is difficult to

[SEARCH]

understand, seeing the strong anisotropy of the medium, why the vertical velocity would dramatically increase the radial resistance. Making a rapid bibliographic research, we could not find any study of the angle incidence between inline and transverse flows. For this reason, the radial pressure loss is transferred into the linear coefficient, however making it proportional to the horizontal speed: $A_r = B_r (v_x^2 + v_z^2)^{1/2}$. In other terms, the horizontal resistance depends only on the horizontal velocity with a quadratic dependence.

5.3 PP

Only momentum thrust is considered for the primary pump. The heat source would have however to be localized.

The pump thrust is localized in an annular section around the PP profiler vertical part. The annulus is 20 cm high for an expected pressure thrust about $dP=2$ Bar giving a force density about $f=10$ Bar/m= $1e6$ Pa/m. However, the exact value of the force is set to equilibrate the flow in nominal condition at the nominal value of 9440 kg/s.

6. Phase control

To avoid unphysical mixing of the two phases, mainly during the filling period, we have to eliminate the light (cover gas) phase at the interface with a source term of the form:

$$S_g = -\text{VolumeFractionPhase1} * \text{VolumeFractionPhase2} / \tau,$$

with the characteristic time taken to $\tau=2$ s.

This source term has also the advantage to create a natural inflow condition at the top numerical stagnation inlet.

To speed up the start-up transient, we have to use the largest possible time step. We therefore have loss of the overall conservation of the LBE mass. This total LBE mass must be monitored and the eventual discrepancy must be corrected by a LBE volume fraction source term. If the objective mass is m_0 and the measured one is m , we set the LBE volume fraction source term S_{LBE} as

$$S_{LBE} = (m_0 - m) / (\rho V \tau)$$

Where V is the volume on which the source is applied and $\tau=10$ s is the usual characteristic return time. The volume fraction source terms can be completed with a related enthalpy term S_h of the form:

$$S_h = \rho * C_p * S_{LBE} * \text{Temperature}.$$

This would be really necessary only if the mass source is large and would otherwise noticeably alter the temperature. We have chosen to localize the mass source in the PP propeller rings.

7. Transient fluid flow simulation to nominal condition

A simulation has been run with the flow initially at rest at cold plenum temperature (270 C). Many adjustments have been performed during this initial transient which are not reported here. Important to note is that while the mass flow rates and free surfaces essentially reach the nominal value in a few tens of seconds, the thermal transient is much more longer, the thermal balance taking more than 2 minutes to equilibrate (up to the IVFS decay heat source). Once

the thermal balance equilibrated up to 5 %, we have run the simulation for 2 additional minutes, to check whether the thermal and velocity field were stable or not. The results presented illustrate these 2 minutes of simulation and the final flow fields.

7.1 Numerical setting

Only the fluid part is simulated, meaning that all walls are treated as adiabatic. The mesh is polyhedral with a prismatic boundary layer, see **Figure 23** right. The main characteristics of the numerical setting is listed below:

- Mesh base size: 7.8 cm (refinement zones at 50%, see **Figure 23** left).
- Cell, face and vertex number: 6.0 M, 33 M, 26 M.
- Time step: 0.01 s.
- Iterations per time step: 4.
- Temporal discretization: 1st order.
- Convection scheme: 2nd order (all equations).
- Turbulence modelling: Realizable Two-Layer K-Epsilon model.
- Volume of Fluid (VoF): sharpening factor 0.1.
- Segregated multiphase temperature.

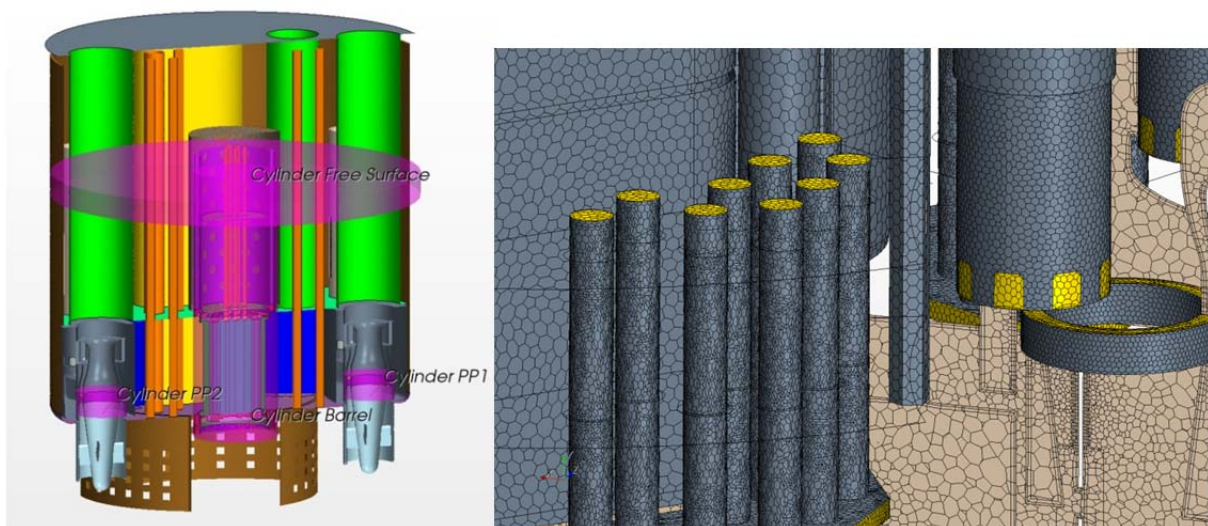


Figure 23. Left: mesh refinement regions. Right: surface/interface mesh detail.

For any missing item in the above list, the default setting of starccm+ has been used. In particular, we have used the default turbulent Prandtl number, value 0.9. Liquid LBE has a very high thermal diffusivity in front with its molecular viscosity and thus has a very low molecular Prandtl number. The result is that a LBE flow may be locally slightly turbulent and still have a thermal molecular diffusivity pattern. There is a range of turbulence, when it is low, in which the molecular and turbulent thermal diffusion compete at a similar scale. In this case, the simple summation of the two effects leads to an overestimation of the global thermal diffusion [14]. To remedy this drawbacks without changing the general equation setting, the simplest and more straightforward approach consists in reducing the turbulent thermal diffusion. This is simply done by increasing the turbulent Prandtl number, either keeping it at a constant value, or making this value depend on the turbulence parameters. For highly turbulent flows, which is our case, the turbulent (unaltered) thermal diffusion stays much

[SEARCH]

higher than the molecular one and a special treatment is not necessary. However, when and if our numerical resolution increases a lot, eventually resolving sufficiently small scales, we will have to take this phenomenology into account.

The mesh can be refined on a geometrical volume basis or on a region basis. The geometrical volumes where the mesh refinement has been applied is shown on **Figure 23**, left. Mesh refinement has also been applied to the regions IVFS and HX porous. A detail of the mesh is shown on **Figure 23**, right.

7.2 Mass flow rates

The evolution during two minutes of the principal mass flow rates are shown on **Figure 24** and the values at time $t=220s$ are given in Table 3.

There is a difference of 143 kg/s between the flow out of the pumps and the flow in outlet of the core. There are three different sources of discrepancy which produce this difference. First, some of the pump flow may still serve to slightly increment the height of the cold free surface. Second, the measure of the flow out of the core is taken at height $h=0.3m$ by setting a derived part surface. The surface does not coincide with the surface of a mesh set and thus some error comes from the projection of the flow field on this derived part. Third, there is a bug in the starccm+ solver which does take into account the density variation when proceeding to the pressure evaluation. The result is that the flow is solved as a Boussinesq flow and due to the core heat power, the flow in outlet is about 90 kg lighter than in inlet. The bug has been submitted to the CD-Adapco developers and is planned to be solved in the release of September 2013 for version 8.04.

The mass flows during the 2 minutes look almost constant and demonstrate a very good global stability. The mass flow rate of the two PPs are very close.

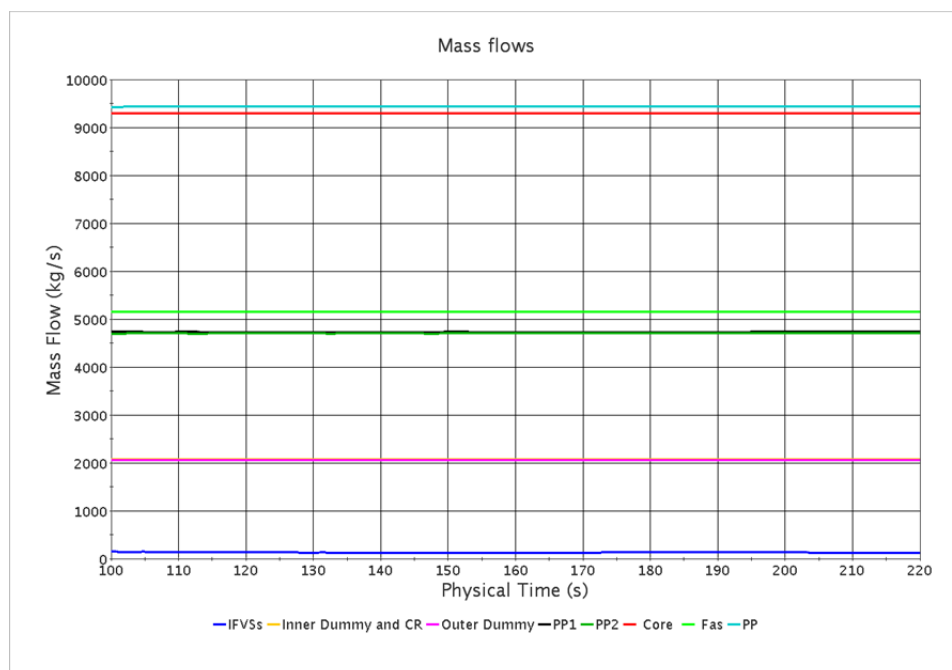


Figure 24: Mass flow rates during the 2 minutes transient.

[SEARCH]

Region	Foreseen mass flow rate [kg/s]	Observed mass flow rate [kg/s]	Relative difference [%]	Comment
Fa	5258	5156	-2.0	After heating
Inner+CR	2103	2074	-1.4	
Outer Dummy	2079	2062	-0.8	
Core	9440	9293	-1.6	After heating
PP1	4720	4735	+0.3	Inlet of PPthrust
PP2	4720	4707	-0.3	Inlet of PPthrust
PPs	9440	9440	0.0	PPthrust outlet
IVFS	-	117		

Table 3: Mass flow rates. Expected values and observed values at time $t=220s$.

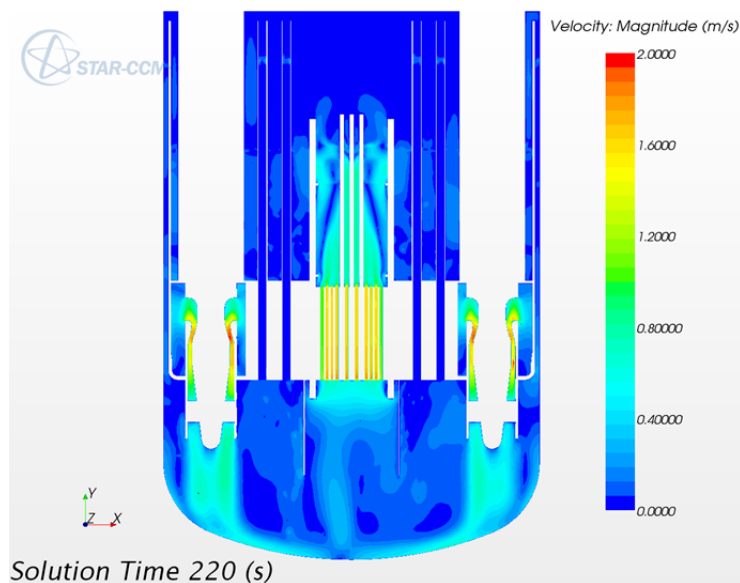
7.3 Velocity field

The velocity modulus field has been monitored during the 2 minutes transient on three planar derived parts.

- The vertical plane passing through the core and the PPs.
- A vertical plane parallel to the first one passing through 2 PHXs.
- An horizontal plane in the cold plenum at level $z=-2.9$ m.

The plots at end of simulation can be seen respectively on **Figure 25**, **Figure 26** and **Figure 27**. On the first figure, on can see a small inconsistency at the right hand side PP level. This is seemingly a numerical inconsistency of the mesh and may be also responsible for the 28 kg/s difference between the two pumps delivery. This difference may also be the cause of the slight decentring of the bottom rising flow towards the core. A noticeable feature of the flow field is that is clearly indicates no stagnant zone at the vessel bottom.

Animations showing the time evolution of the velocity field on the three chosen plane have been produced. They show a quite stable, slowly evolving field in the lower and the upper plenum. The only region showing fast changes is the upper part of the PHXs. Fortunately, this instability does not propagate downstream inside the PHXs.



[SEARCH]

Figure 25: End of the 2 minutes simulation. Velocity modulus field on a vertical plane passing through the core and the PPs.

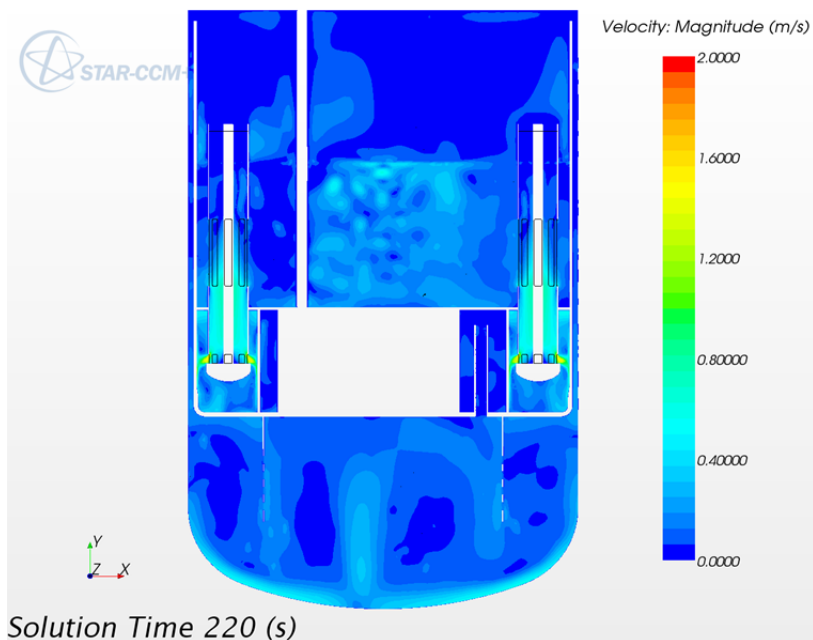


Figure 26: End of the 2 minute simulation. Velocity modulus field on a vertical plane passing through two PHXs.

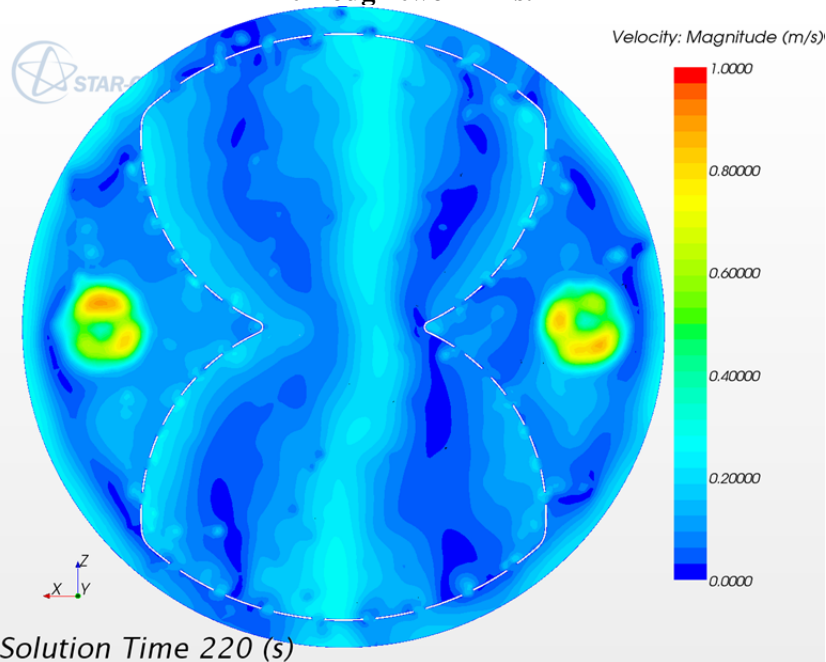


Figure 27: End of the 2 minute simulation. Velocity modulus field on a horizontal plane at quote $y = -2.9$ m.

7.4 Thermal field

The thermal field has been monitored during the 2 minutes transient on 5 derived parts:

- The surface temperature
- The isotherm 350 C surface

[SEARCH]

- The vertical plane passing through the core and the PPs.
- The vertical plane passing through the core and the IVFH
- A vertical plane passing through the PHXs.

The corresponding plots are shown respectively on **Figure 28** to **Figure 32**. When necessary, the temperature indicated has been modified to clearly separate the cover gas region which is of no interest in this analysis. The Temperature shown in these case is the usual temperature multiplied by the ratio of mixture density to the LBE density, which in fact is not so different than the usual temperature multiplied by the LBE volume fraction. The former is preferred because it may be also useful to use the inverse ratio which would become undefined using the LBE volume fraction in the far cover gas.

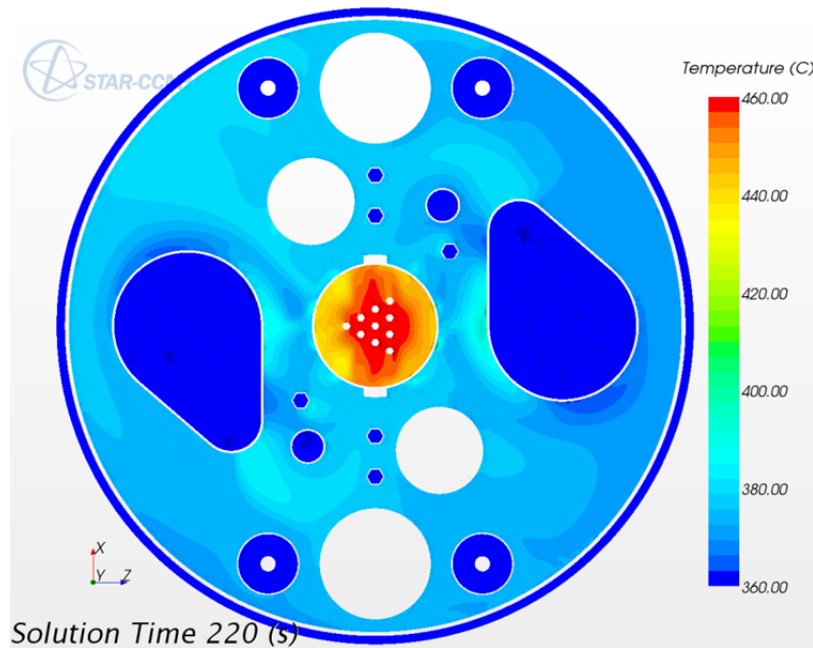


Figure 28: End of 2 min simulation. Free surface temperature.

The free surface inside the Core Barrel is just below one ring of holes. The free surface outside the Core Barrel is just over the next ring of holes. The result is that the Core Barrel creates a very stiff separation between the two free surface temperatures. The Free surface temperature is not very symmetrical. This is possibly due to the asymmetry of the three SR positions, two on the right side and one on the left side (x-axis pointing on the right). The hot flow is then slightly unbalanced leading to a free surface slightly hotter on the left side.

The figures indicates a quite articulated but clear thermal stratification. The isotherm at 350 C is a connected surface. This is an indicator of stability of the stratification.

The stability of the stratification is much better checked by visualizing the animations of the 2 min transients on the five surfaces. It results that the central region, say, between the two IVFH penetrations is almost stationary. The peripheral region however still slightly evolves during the transient. This is consistent with the slight evolution of the temperature in inlet of the PHXs. The only clearly instable region is the upper part of the heat exchanger over the inlet level. This is clearly a buoyancy driven instability as the temperature in this region tends to become much colder than the incoming flow from below. The instability however does not propagate downstream into the PHXs.

It is possible for some part of the stratification to be unstable, as the isotherm is locally not the graph of a function over the horizontal plane (it would be a multi-valued function). Should these parts be unstable, this would be on a time scale larger than the minute.

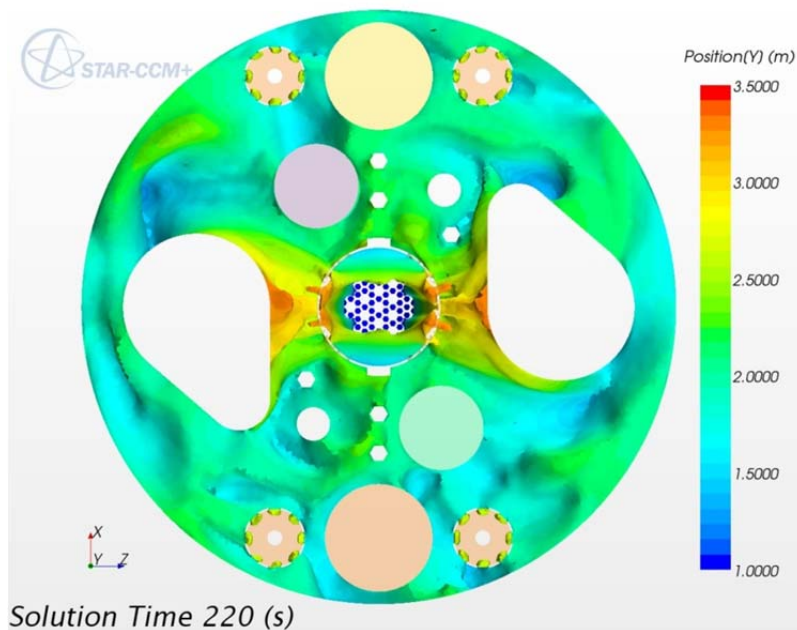


Figure 29: End of 2 minutes simulation. Isotherm $T=350$ C in LBE, coloured by height.

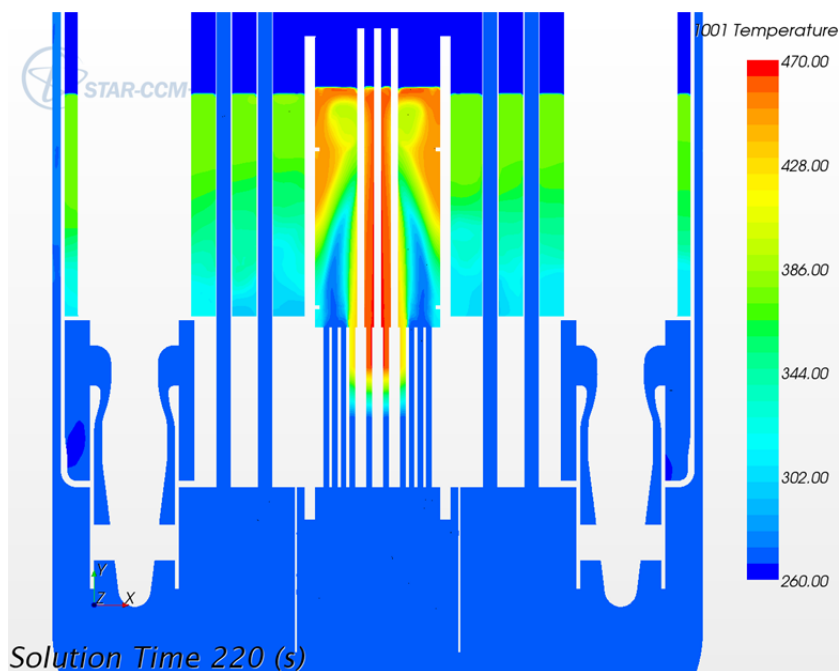


Figure 30: End of 2 min simulation. Temperature field on the plane passing through the core and the PPs.

[SEARCH]

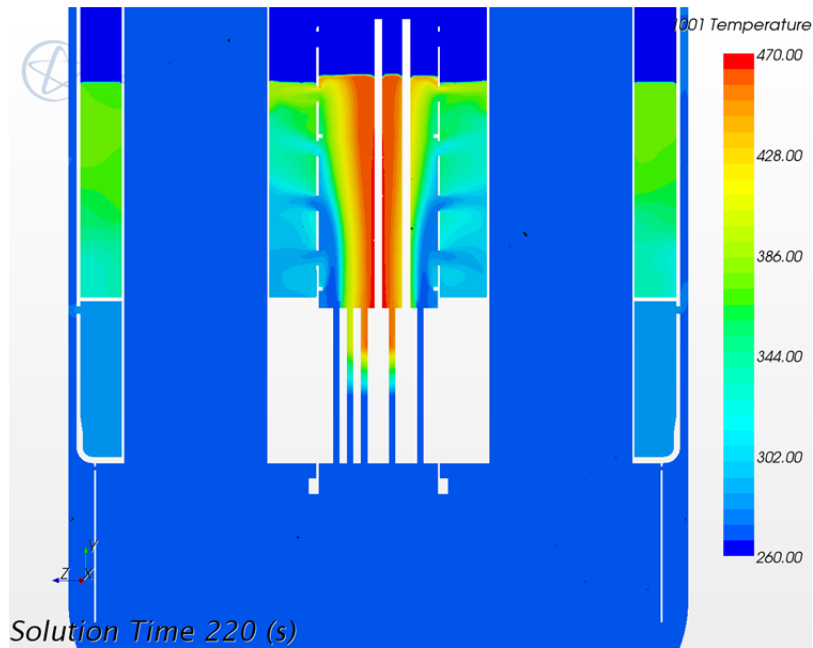


Figure 31: End of 2 min simulation. Temperature field on the plane passing through the core and the IVFHs.

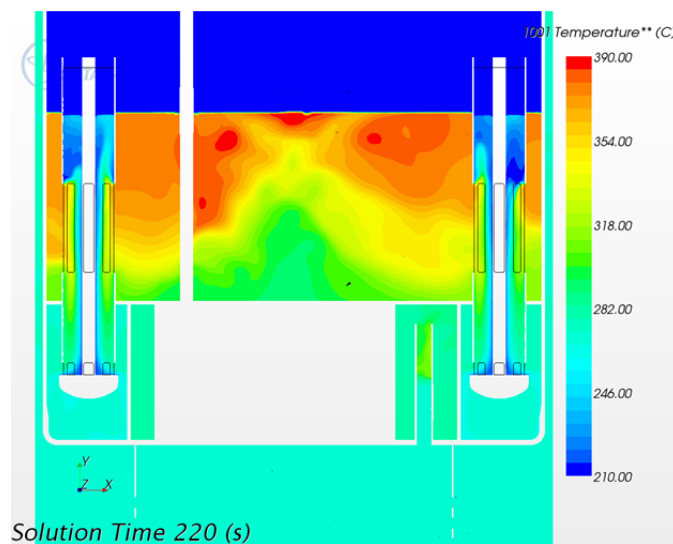


Figure 32: End of 2 min simulation. Temperature field on the plane passing through two PHXs.

7.5 Thermal balance

The flux mean temperature has been monitored in inlet and outlet of the PHXs. The temperatures evolution during the 2 minutes transient is shown on Figure 33 while the PHX power evolution is shown on Figure 34. The inlet temperature is still slightly increasing towards the expected intermediate asymptotic temperature of 342 C. At time $t=220s$, the inlet temperature is 341.8 C and the outlet temperature is 270.3 C. Consistently with the temperature evolution, the PHX power slowly converges to 100 MW. The discontinuity of the curve at time 175s is due to a slight change in the characteristic time of the heat source term, in order to keep the outlet temperature near 270 C.

[SEARCH]

The thermal balance shows that we are about 3% away from (the intermediate asymptotic) equilibrium at the beginning of the 2 minutes simulation and only 0.5 % away from it at the end of the simulation. The end of the simulation is therefore a good candidate for a converged stationary solution to be used as initial field for further transients, normal and incidental.

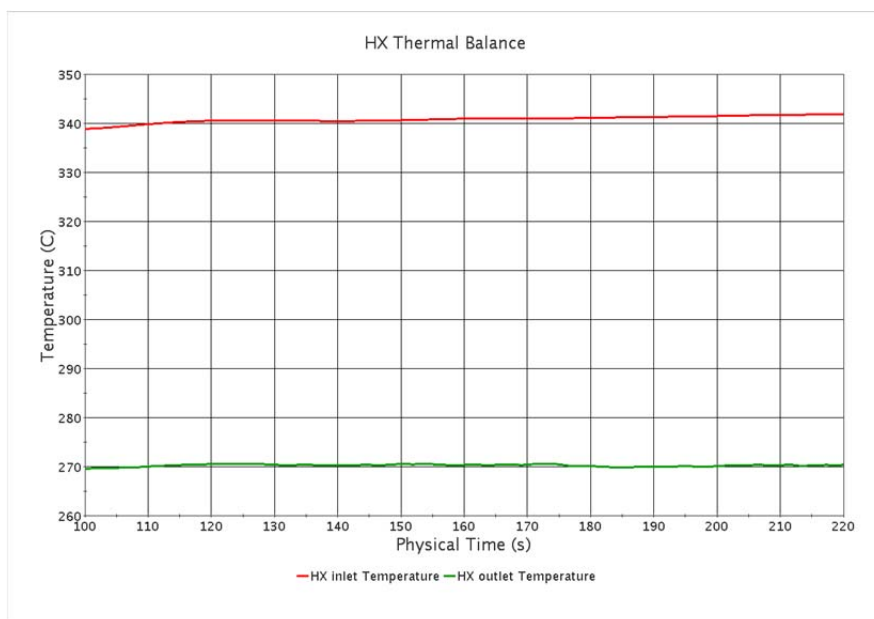


Figure 33: Time evolution of the temperature in inlet and outlet of the PHXs.

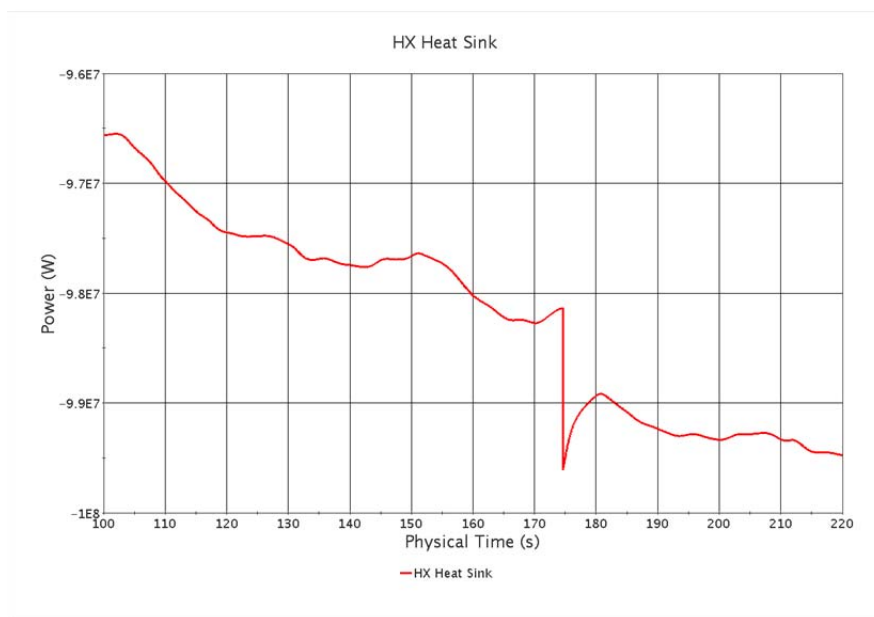


Figure 34: Time evolution of the heat power transferred to the PHX.

8. Conjugate heat transfer simulation

The main drawback of the former model is that it lacks the effect of the structure. A new model has thus been built including the main structural parts.

[SEARCH]

8.1 Updated model

Two additional materials have been defined:

- AISI 316L stainless steel for the structures, shown on Figure 35. The former isolated volume around the Fa positions is strongly approximated to be of this material and is merged with the rest of the main structure. The external vessel is given its own separated region because only this part needs a radiating heat flux treatment.
- “Solid LBE” for the dead volume around the core, shown on Figure 35, right. This solid has the same physical properties of the LBE, but is treated as solid. This allows to deal with the density dependence on temperature in a closed domain without risking to have a blow up in pressure due to the incompressibility constraint. Solid LBE has the same enthalpy of LBE. If, in a future version of the model, the bypass gaps are reintroduced, we hope that a restart of the solution with the solid LBE domain converted to a normal liquid LBE domain can be manageable.

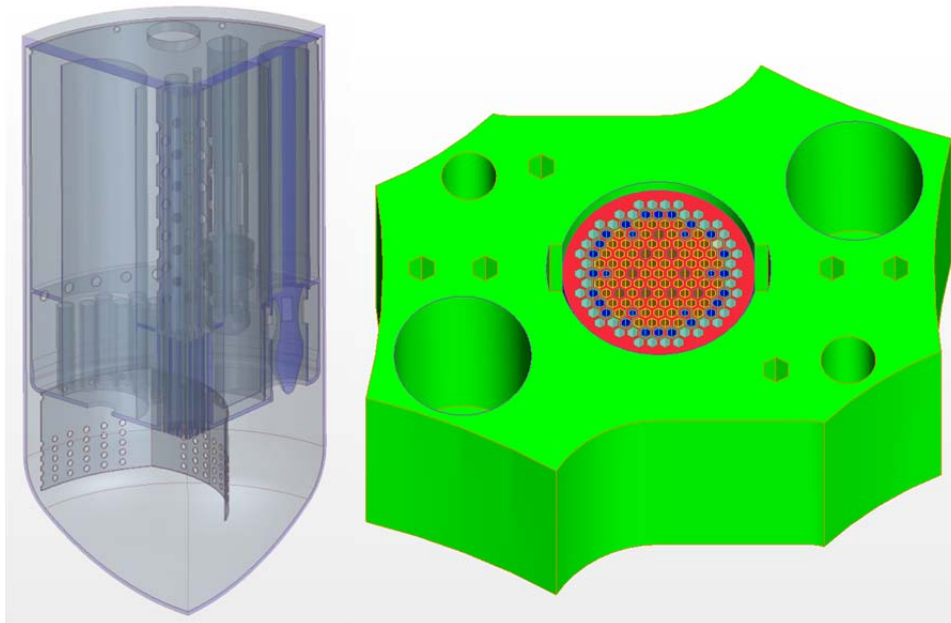


Figure 35. Left: solid domain. Right: in green, geometry of the LBE dead volume; In red, the solid part of the core.

The model has been upgraded to the version 8.02 of the software. The complete geometry has been completed and slightly corrected to have full consistence between the fluid domain and the solid domain. The mesh base size has been slightly reduced from 7.8 cm to 7.2 cm. The refined mesh has been extended in the PP region, as shown in **Figure 36**, left. The entire mesh has been built using 9.3 million control volumes (8.3 million for the LBE, 1.0 million for the structure and 65 thousands for the dead volume), 52 million interior faces and 49 million vertices. A detail of the mesh is shown on **Figure 36**, right.

The solution of the precedent model has been projected on the extended domain. The structure temperature and the solid LBE temperature have been initialized at 270 C, the cold flow temperature.

[SEARCH]

The vessel external wall exchanges heat with its surrounding by grey body irradiation with emissivity of 0.6 supposing an incident flux from the outside wall at 300 K. Numerically, a temperature dependant heat flux is imposed on the external wall with value in W/m^2 :

$$\phi = 0.6 \sigma (T^4 - T_0^4)$$

with $T_0 = 300K$ and the Stefan-Boltzmann constant $\sigma = 5.67E-8 W/m^2/K^4$.

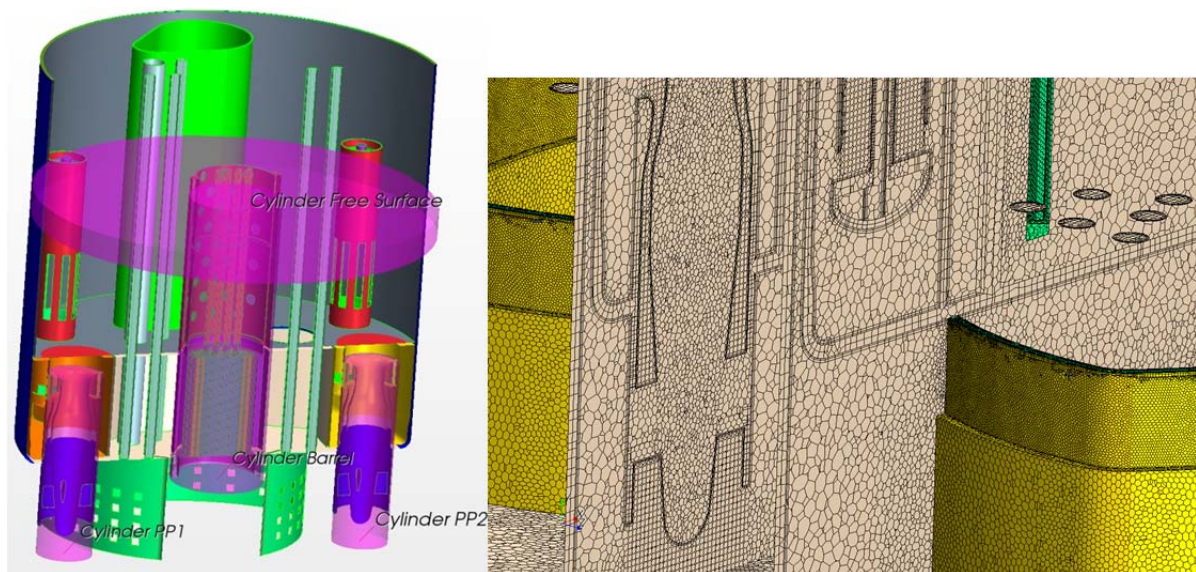


Figure 36. Left: Geometry with the refinement zone of the 9.3 E6 cell mesh highlighted. Right: mesh detail.

On the consistency between the temperature density variation and the incompressibility constraint, a workaround has been found, setting the density change as user defined and no more as polynomial. The mass flow across the core is now correctly conserved.

With the CRS4 cluster operative system update (Centos) and the software update to version 8.02, we have been able to run the simulation in parallel on up to 256 cores and effectively run up to 25s of transient per day of simulation.

The characteristic time of the temperature diffusion equation is for steel: $\tau = L^2 \rho C_p / k \approx 2.7E5 L^2$. This gives 1800s for the external vessel (8 cm wide) and 700s for the internal vessel (5 cm wide). These numbers give an idea on how long it takes for the structure to raise in temperature with fixed boundary conditions. But the boundary conditions are not fixed. The LBE volumes in the “cold” plenum above the core level are almost stagnant regions and will be slowly heated by the conducting wall. This process is likely to take hours to reach a new equilibrium and therefore is unreachable under the conditions of a normal transient. A foreseen expected workaround was to freeze the flow and run only the temperature equation. This is a standard procedure but it cannot be applied yet to our case, seemingly because of the VOF implementation. Trials to proceed led to a fast unphysical increase of temperature at the LBE surface, rapidly spoiling all the simulation.

8.2 Results

The simulation has been restarted for 150s to readjust the velocity field and partially the thermal field. The results of this simulation is not illustrated and is only shortly commented here. Numerically, the change in mesh density is rapidly absorbed. Only the cover gas velocity field is perturbed for a few tens of second. This is due to a very touchy rebalancing of

[SEARCH]

the momentum and pressure at the free surface during the projection of the fields from the old onto the new mesh. The most dramatic effect is on the thermal field as the fluid heats the structure bounding the hot plenum. The result is a cooling of the hot plenum and the HX power decreases up to 10%, before restarting slowly to increase. During this time the HX power is strictly kept under control to avoid excessive deviation of the outlet flow temperature towards the cold plenum.

The last simulation reported here is the prosecution of the former one for 300s more.

8.2.1 Thermal field

During the 300s simulation, the HX power slowly returns towards the intermediate asymptotic of 100 MW, reaching nearly 97 MW at the end of the simulation, see **Figure 37**. The HX inlet temperature increases slowly towards the expected 342 C but staying below 340 C (reaching 338 C) as the heating of the cold plenum annulus and of the IVFH penetrations will last for a much longer time, see **Figure 38**. The discontinuity at time 150s is due to a slight change of the heat sink characteristic time to keep the outlet temperature about 270 C. In the meantime, the structure temperature slowly equilibrates with the surrounding fluid temperature.

We have monitored the heat flux both sides of the external vessel and of the internal vessel. This is to investigate if the flux across the structures reaches equilibrium both internally and externally. The time history of the heat flux is shown on **Figure 39**. The heat flux converges very slowly towards the equilibrium value and is still quite far from it at the end of the simulation. The temperature on both sides of the Vessel is shown on **Figure 40**. The vessel external side has cooled down by nearly 8 degrees in 450s. The internal side begins to feel the effect of the slightly hotter fluid in the cold plenum upper annulus. This is consistent with some a priori estimates that we have done before.

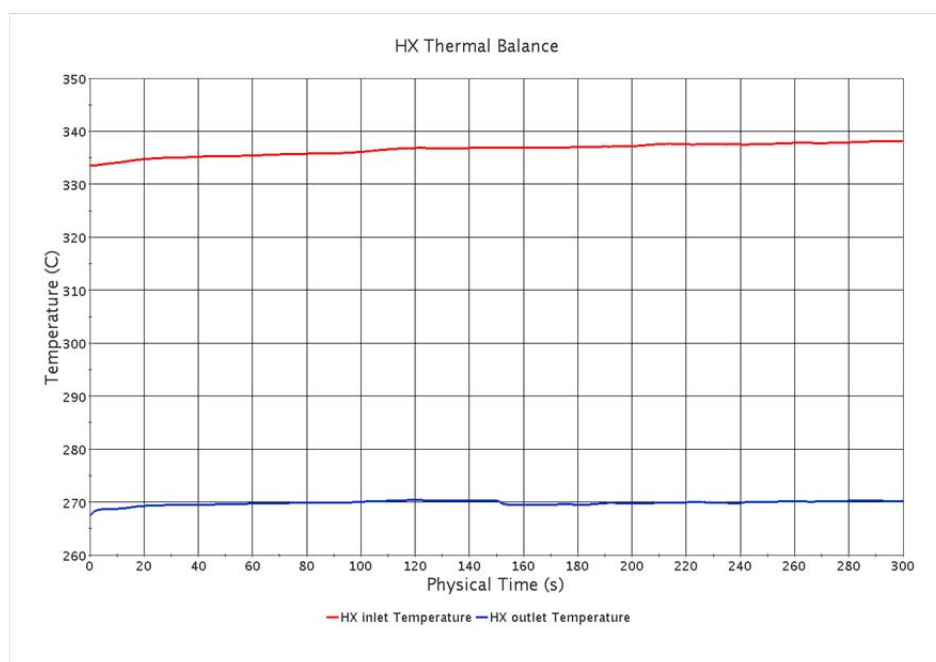


Figure 37: Mean flow temperature in inlet and in outlet of the HXs

[SEARCH]

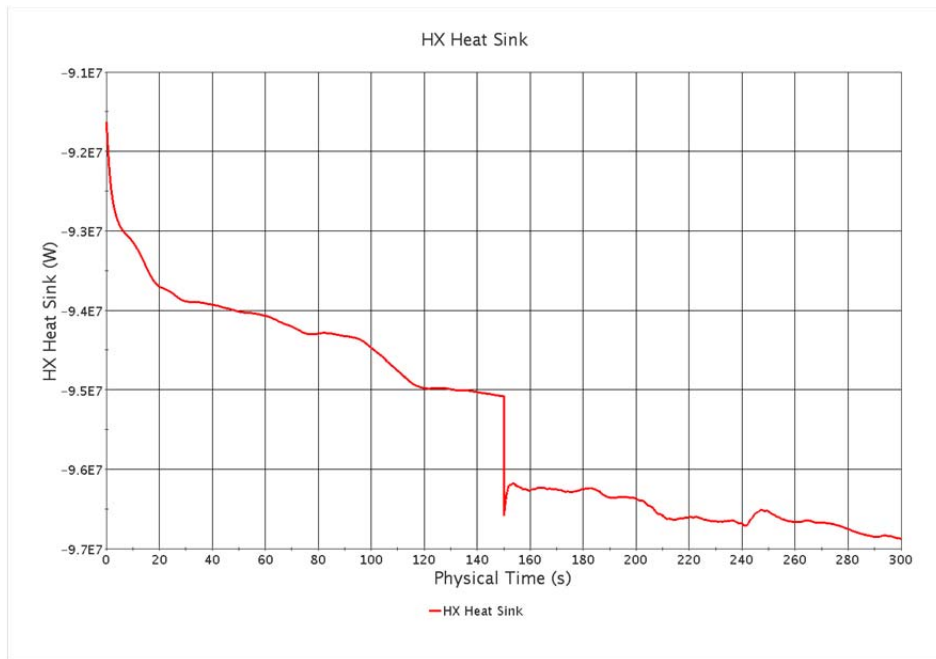


Figure 38: history of the HX power.

The temperature field at the end of the 300s simulation is reported on three vertical planes, passing (i) through the PPs and the core, **Figure 41** left, (ii) through the IVFHs and the core, **Figure 41** right and (iii) through two HXs, see **Figure 42**. The temperature field in the hot plenum is very similar to the one in the previous model. The temperature in the cold plenum is slightly changed as the conjugate heat transfer begins to be felt, in the upper external annulus and in the various vertical penetrations. The decay heat in the IVFS is now clearly noticeable. Looking at the fluid temperature in the IVFH, it is clear that the heating process is only at its beginning. The temperature in the HX is much more articulated, mainly because the mesh resolution here has been slightly improved. As before, the temperature field is unstable above the inlet and stable below it, as can be clearly seen on the transient animation. The transient animation related to **Figure 41** right shows a slight flickering of the thermal profile above the core. This flickering is not present on the orthogonal plane.

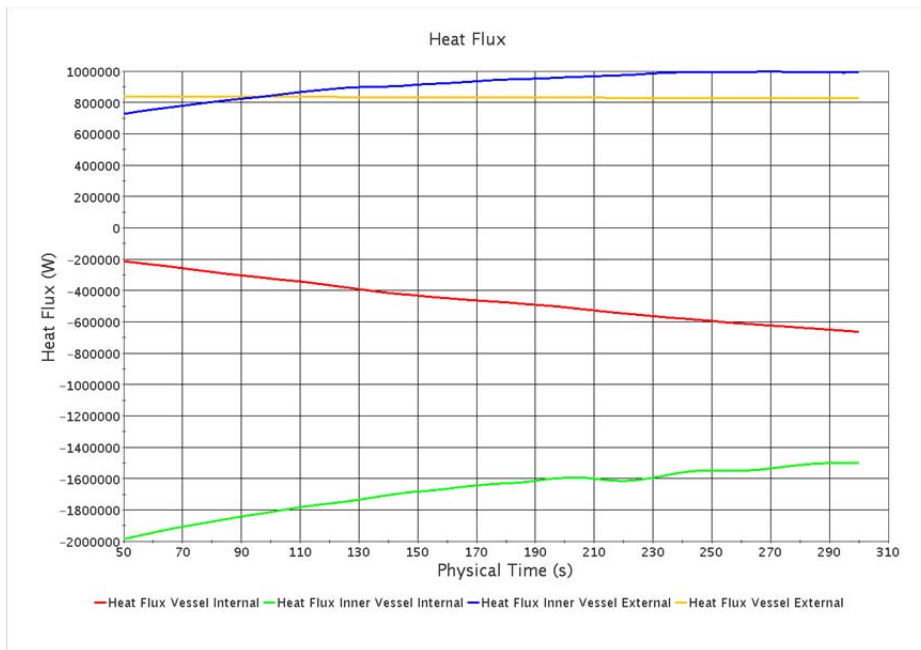


Figure 39: heat flux 300s history for both sides of the external and internal vessels.

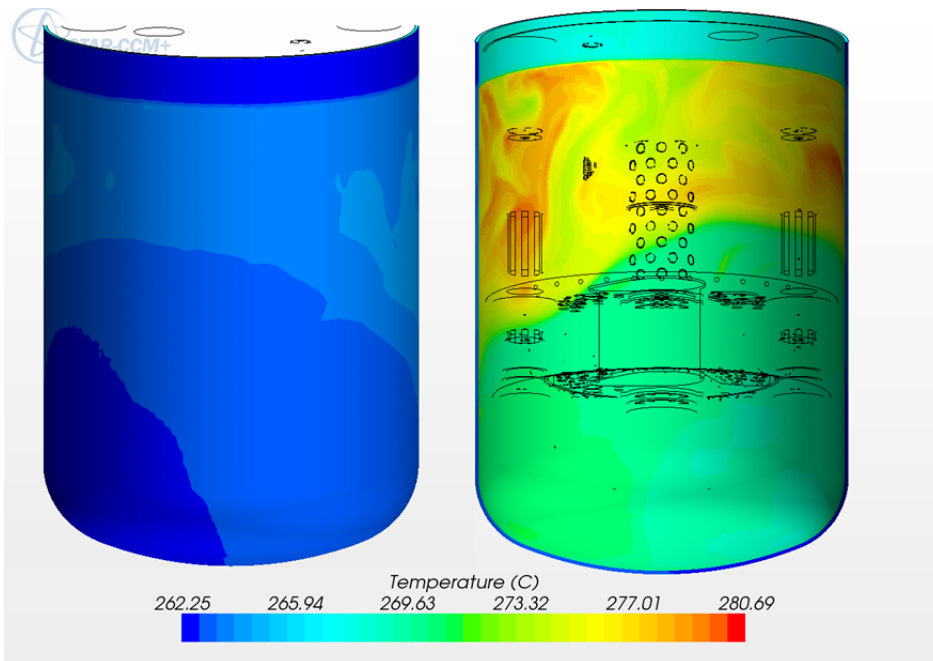


Figure 40: temperature field on both sides of the Vessel at simulation end.

[SEARCH]

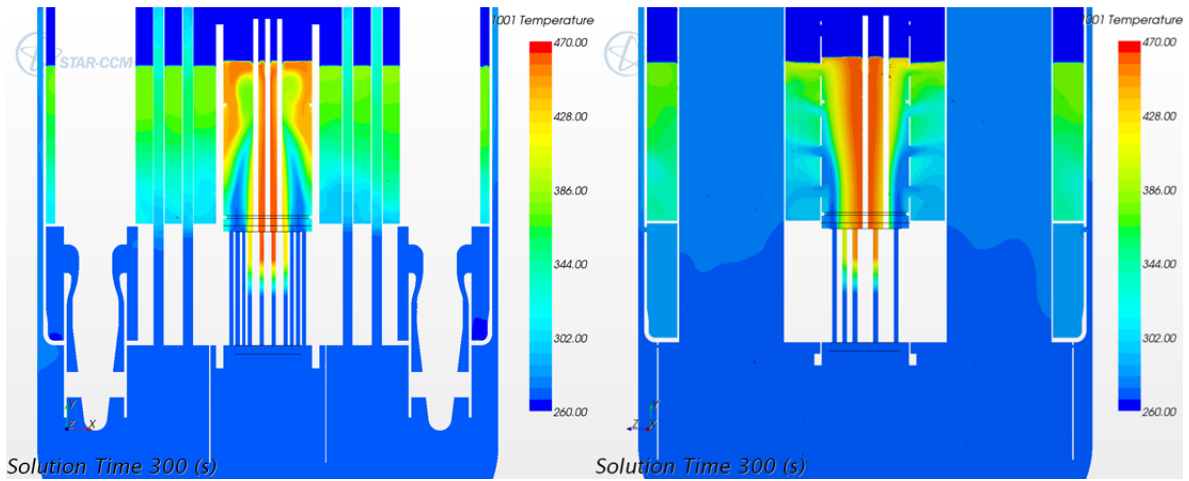


Figure 41: thermal field on two orthogonal planes centred on the core.

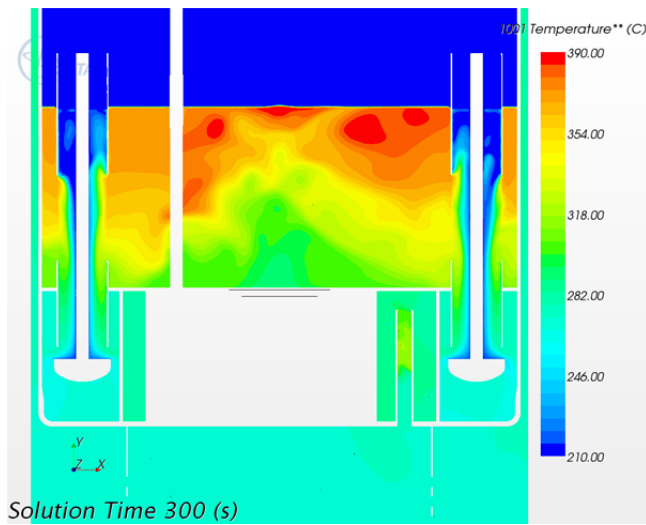


Figure 42: thermal field on a vertical plane linking two HXs.

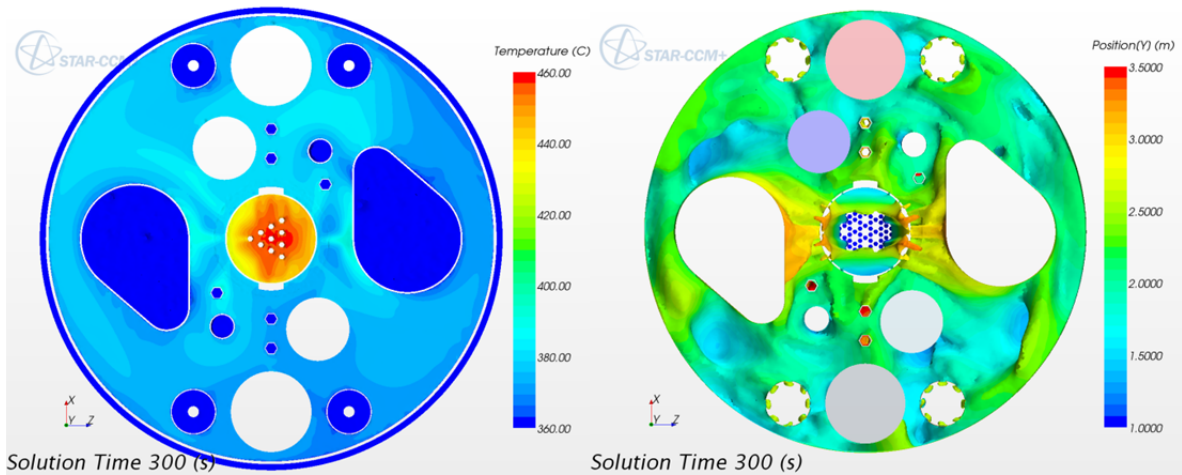


Figure 43: thermal field. Left, surface temperature. Right, iso-surface at 350 C coloured by vertical quote.

[SEARCH]

8.2.2 Velocity field

The velocity field in the hot plenum is nearly stationary, at least in the two vertical planes observed and shown in **Figure 44**. We noticed however an un-stationary flow behaviour in the main cold plenum and in the HX above the inlet level. Most noticeably, while the right PP outlet flow is quite regular, the left one is strongly perturbed. The result is a slightly variable mass flow rate in the right PP (PP1 in **Figure 46**) which is also slightly lower than the left PP flow rate, see the two lines in the range 4500-5000 kg/s in **Figure 46**. The small oscillations of the PP mass flow rate does not affect the core mass flow rate. The free surface thus acts as a dampening buffer. In confront with the former model, the mesh resolution below the PP has been greatly improved and thus the flow instability is likely to have a physical origin.

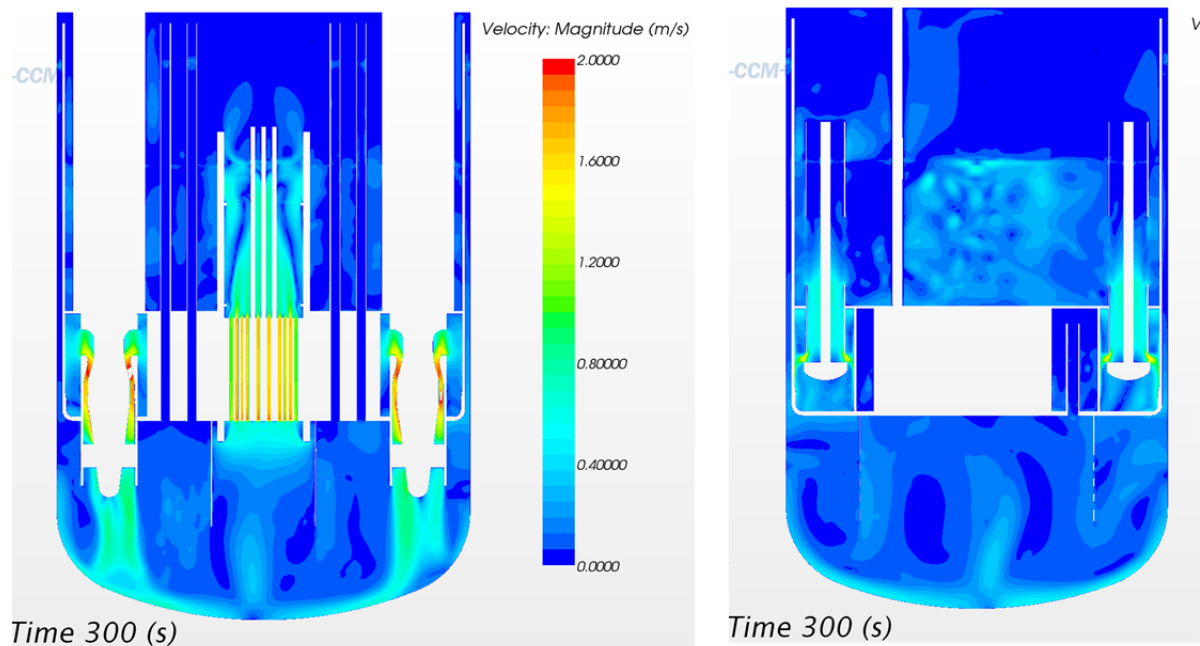


Figure 44: field of velocity magnitude. Left, vertical plane passing through the PPs. Right, vertical plane passing through two HXs.

[SEARCH]

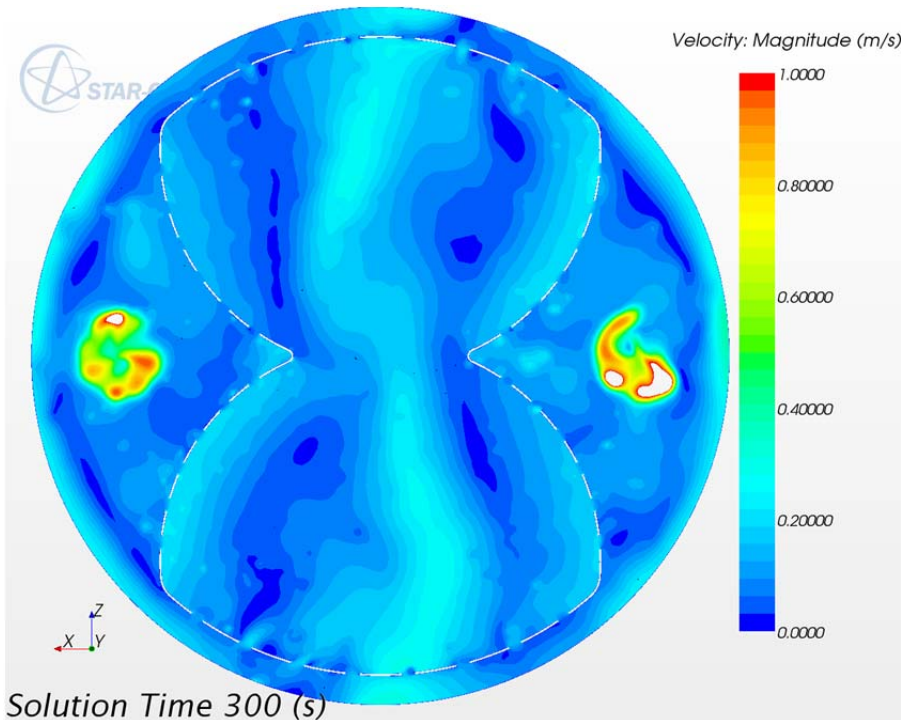


Figure 45: field of velocity magnitude on the horizontal plane at quote $y=-2.9m$.

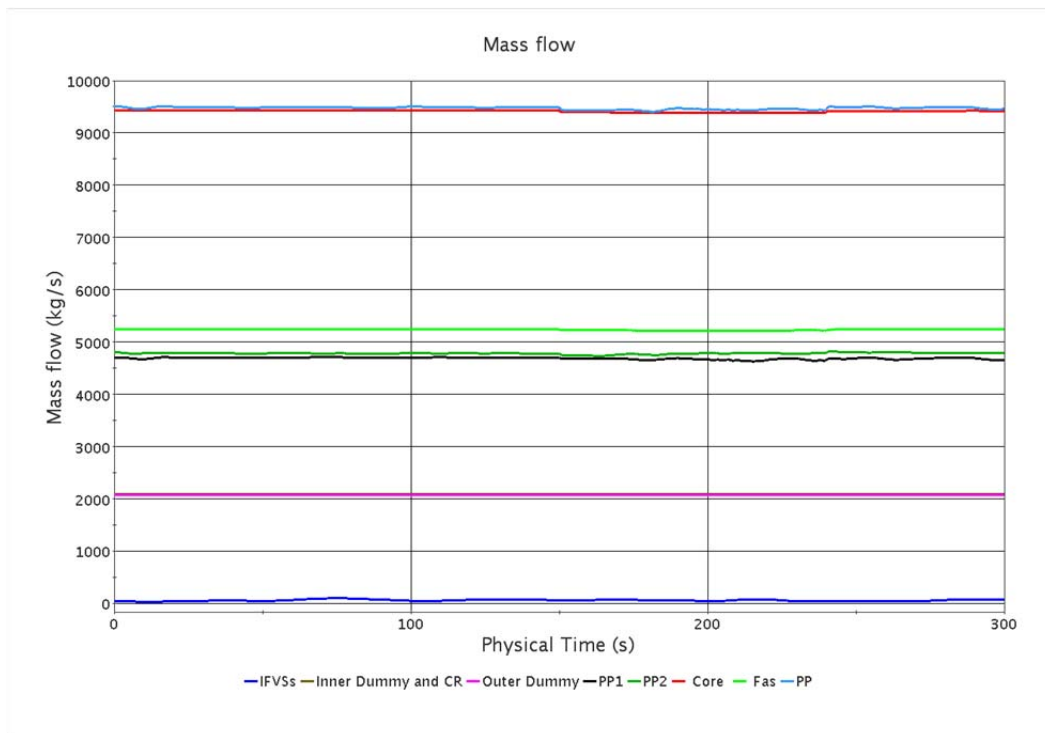


Figure 46: principal mass flow rates

[SEARCH]

9. Concluding word

A CFD representation of MYRRHA primary system with 6 million control volumes has been built. This representation includes the free surface dynamics but not the thermal exchange with the structural parts. The model has been run in transient mode and comes very close to the nominal operation. The stability of the flow in nominal condition has been checked by monitoring some velocity and temperature fields during 120 seconds. The flow seems quite stable in the hot plenum where it is subject to a strong thermal stratification. The flow gently oscillates in the cold plenum thus avoiding the presence of stagnation zones at the bottom. The model can be used as initial condition for the next part of the work package, that is, the fuel dispersion study. The objective of the deliverable can thus be considered to be successfully reached.

A second CFD representation of MYRRHA primary system with 9.3 million control volumes has been built. This representation also includes the conjugate heat transfer with the structural part, dealt with 1 million control volumes. The mesh density is slightly increased, passing from 7.8 to 7.2 cm base mesh size (27 % denser) and further increasing the refined regions. This augmented model however is subject to the time scale of the temperature diffusion through the solid structure. The result is a greater thermal inertia and a strongly increase of the time necessary to reach a reasonably stabilized thermal profile. While the stabilized thermal profile of peripheral regions is not reachable with the available computational power, it is almost reached in the main flow circulation path. The increased mesh definition has raised the flow pattern less stable, mainly in the cold plenum which is essentially not subject to thermal stratification. A flow instability in outlet of one PP is observed.

While the second CFD representation of MYRRHA primary system is a decisive improvement in confront with the former representation, it may be not better suited to the primary objective of this work which is the fuel dispersion study. In effect, the un-stationary behaviour of the cold plenum flow makes questionable the classical approach consisting in releasing bunches of Lagrangian particles in a frozen flow. This problematic will be affronted in the successive part of the work package.

References

- [1] <http://myrrha.sckcen.be>
- [2] F.Bianchi et al., Thermo-hydraulic analysis of the windowless target system, Nuclear Engineering and Design, Volume 238, Number 8, page 2135--2145 - august 2008.
- [3] V. Moreau et al., A case history of cfd support to accelerator driven system plant design, Proceedings of The 17th Int. Conf. On Nucl. Eng num. 75588 ASME – 2009.
- [4] V. Moreau, FASTEF Heat exchanger tube rupture CFD simulation, Nuclear Engineering and Design Elsevier pages 42-51 vol. 252 - 2012 doi: <http://dx.doi.org/10.1016/j.nucengdes.2012.06.030>
- [5]<http://www.inl.gov/relap5/>
- [6] <http://www.jaea.go.jp/inc/zooarai/ejooarai/simmer/>
- [7] MYRRHA Team, “MYRRHA Technical Description Rev. 1.2”, <http://search.sckcen.be/>, February 2012.
- [8] MYRRHA Team, “MYRRHA Technical Description Rev. 1.4”, <http://search.sckcen.be/>, June 2012.
- [9] N. Forgione et al. Operability of the SIMMER-III and SIMMER-IV models for the MYRRHA-FASTEF reactor, SEARCH contractual deliverable D5.1 (Contract Number: 295736),12/2012.
- [10] <http://www.cd-adapco.com/>.
- [11] Handbook on Lead-bismuth Eutectic Alloy and Lead Properties, Materials Compatibility, Thermal-hydraulics and Technologies, Nuclear Energy Agency 2007 Edition <http://www.nea.fr/html/science/reports/2007/nea6195-handbook.html>
- [12] <http://search.sckcen.be/>
- [13] <http://www.atlassteels.co.nz/site/pages/technical-handbooks-of-stainless-steel.php>
- [14]M. Manconi, “Investigation of the near-wall modelling strategy and the concept of the turbulent Prandtl number for low Prandtl number flows”, master thesis UCL, 2012. Belgian Nuclear Higher Education Network (BNEN).

Appendix: List of user functions reports and plots

Many user functions must be defined to setup the simulation. They can usually be applied on a region basis. Forces and source terms require the definition of their derivative by the reference variable for a better numerical treatment of non-linear terms. The derived functions are indicated with “d” as first letter. Here is a complete reminder list (initial number used to order it):

[SEARCH]

- 100 Unit: to calculate volumes and surfaces
- 101 Unit below 3.97: to calculate immersed volumes
- 102 R: Radius for PP swirling force
- 103 Theta: angle for PP swirling force
- 110 Initial Volume Fraction Phase 1
- 120 Initial Volume Fraction Phase 2
- 130 Initial Pressure
- 200 LBE Density
- 210 LBE viscosity
- 220 LBE Conductivity
- 221 Steel Conductivity
- 310 Vertical HX Linear resistance coefficient
- 311 Vertical HX Quadratic resistance coefficient
- 320 Horizontal HX Linear resistance coefficient
- 321 Horizontal HX Quadratic resistance coefficient
- 330 Vertical ACS inertial resistance coefficient
- 340 Horizontal ACS inertial resistance coefficient
- 410 Core Fa resistance
- 411 Core Fa resistance derivative
- 420 Core Outer Dummy resistance
- 421 Core Outer Dummy resistance Derivative
- 430 PPforce
- 510 HXsink
- 511 dHXsink
- 520 IVFS Heat Source
- 530 Core Fa Heat source
- 540 Numerical Top Heat Source
- 550 Radiative Heat Flux
- 610 Vertical Mass flow rate: for report on core
- 620 Downward mass flow rate: for report on HXs
- 710 relative LBE density: for report on total LBE mass

[SEARCH]

Deliverable 5.3 – [Two-phase CFD model of the MYRRHA-FASTEF primary coolant loop including all relevant thermal aspects](#)

Dissemination level: [PU](#)

Date of issue of this report: [04/12/2013](#)

48/50

- 810 VF_sharp: for free-surface sharpening
- 820 Mom_sharp
- 821 dMom_sharp
- 830 Energy_sharp
- 831 dEnergy_sharp
- 840 K_sharp
- 841 dK_sharp
- 850 Eps_sharp
- 851 dEps_sharp
- 910 MassCons VF: for global mass conservation
- 920 MassCons Energy
- 921 dMassCons Energy
- 1000 Temperature*: temperature for isotherm filtering the free surface
- 1001 Temperature**: temperature filtering the cover gas

Here is the list of report prepared, sometimes making use of the user functions:

- Heat Transfer Inner Vessel External
- Heat Transfer Inner Vessel Internal
- Heat Transfer Vessel External
- Heat Transfer Vessel Internal
- HX Heat Sink
- LBE total mass: volume integral of function 710
- Mass Flow Averaged T PP: mean temperature in inlet of the PP thrust region
- Mass flow rate through core
- Mass flow rate through Fas
- Mass flow rate through IFVs
- Mass flow rate through Inner Dummy and CR
- Mass flow rate through PP
- Mass flow rate through PP left
- Mass flow rate through PP right
- Mass flow rate through Outer Dummy

[SEARCH]

- T HX in: mass flow averaged temperature of the mixture entering the HXs from upper plenum.
- T HX out: mass flow averaged temperature of the mixture leaving the HXs at the bottom
- Volume Integral Heat Source FAs: for initial normalisation
- Volume Integral Heat Source IVFS: for initial normalisation
- Volume Integral LBE
- Volume Integral Surface Sharpening: to monitor the free-surface volume.

[SEARCH]

Deliverable 5.3 – [Two-phase CFD model of the MYRRHA-FASTEF primary coolant loop including all relevant thermal aspects](#)

Dissemination level: [PU](#)

Date of issue of this report: [04/12/2013](#)

50/50

Degrève Margot

From: Schuurmans Paul
Sent: woensdag 4 december 2013 11:42
To: Degrève Margot
Subject: FW: 295736 - SEARCH - Acknowledgement of Receipt of submitted deliverable Two-phase CFD model of the MYRRHA-FASTEF primary coolant loop including all relevant therm 5.3

From: European Commission [mailto:no-reply@ec.europa.eu]
Sent: woensdag 4 december 2013 10:51
To: Schuurmans Paul
Subject: 295736 - SEARCH - Acknowledgement of Receipt of submitted deliverable 5.3 Two-phase CFD model of the MYRRHA-FASTEF primary coolant loop including all relevant thermal aspects

Europa / Research / Participant Portal notification

European Commission
Research and Innovation DG
Brussels
Belgium

Subject: 295736 - SEARCH - Acknowledgment of Receipt (D5.3:Two-phase CFD model of the MYRRHA-FASTEF primary coolant loop including all relevant thermal aspects)

Dear Coordinator,

Thank you for submitting a scientific deliverable for the project 295736 - SEARCH.

Your scientific deliverable (Two-phase CFD model of the MYRRHA-FASTEF primary coolant loop including all relevant thermal aspects) has been received by the European Commission - Research and Innovation DG.

Please note that this acknowledgement of receipt does not imply that your deliverable is complete or accepted.

Where appropriate, you will be contacted in due course by your contact person(s) in the European Commission - Research and Innovation DG.

The submitted deliverable has been registered as document Ares(2013)3634826.

This Acknowledgement of Receipt has been registered as document Ares(2013)3634829.

Yours sincerely,
European Commission - Research and Innovation DG

This is an automatic email generated by the Scientific Reporting Notification System of the Participant Portal. Please do not reply.